NASA TECHNICAL MEMORANDUM NASA TM-76443

SCATTER OF X-RAYS ON POLISHED SURFACES

G. Hasinger

Translation of Die Streuung von Roentgenstrahlen an Polierten Oberflaechen, Max Planck Institute for Physics and Astrophysics, Institute of Extraterrestrial Physics, Garching bei Muenchen, West Germany, report MPI-PAE/Extraterr. 163, May 1980, pp 1-65

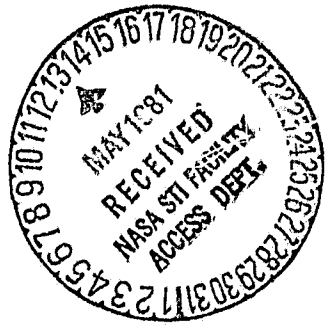

NATIONAL AERONAUTICS AND SPACE ADMINISTRATION
WASHINGTON, D. C. 20546 January 1981

STANDARD TITLE PAGE

1. Report No.	2. Government Accession No.	3. Recipient's Catalog No.
NASA TM-76443		

4. Title and Subtitle	5. Report Date
SCATTER OF X-RAYS ON POLISHED SURFACES	JANUARY 1981
	6. Performing Organization Code

7. Author(s)	8. Performing Organization Report No.
G. HASINGER	10. Work Unit No.

9. Performing Organization Name and Address	11. Contract or Grant No.
SCITRAN Box 5456 Santa Barbara, CA 93108	NASw-3198
	13. Type of Report and Period Covered
	Translation
12. Sponsoring Agency Name and Address National Aeronautics and Space Administration Washington, D.C. 20546	14. Sponsoring Agency Code

15. Supplementary Notes

Translation of Die Streuung von Roentgenstrahlen an Polierten Oberflaechen, Max Planck Institute for Physics and Astrophysics, Institute of Extraterrestrial Physics, Garching bei Muenchen, West Germany, report MPI-PAE/Extraterr. 163, May 1980, pp 1-65

81N-19701

16. Abstract: Subsequent to World War II, the x-ray region of the electromagnetic spectrum began to be used for investigating previously unknown phenomenon.

In 1960 a mirror system for use in x-ray astronomy was adopted.

These new techniques imposed stringent demands on the dispersion properties of the telescope mirror.

This study investigates the scattering characteristics of various surfaces and the mathematics involves in such determinations.

Approximately 60 equations, 35 Figures/Tables and 26 References are contained.

17. Key Words (Selected by Author(s))	18. Distribution Statement
	Unclassified - Unlimited

19. Security Classif. (of this report)	20. Security Classif. (of this page)	21. No. of Pages	22. Price
Unclassified	Unclassified	58	

TABLE OF CONTENTS

Introduction

/2*

During more than 300 years of observing the heavens with the telescope, only optical astronomy has explored the universe. However, in the second third of our century astronomy has acquired new eyes for observing the cosmos. The development of radioastronomy and later the advent of space travel have opened up unexpected regions of the electromagnetic spectrum and have made astronomy less dependent or the optical window into the universe.

The first step was taken by Jansky in 1931 when he discovered the ultrashortwave radiation from the Milky Way while seeking the source of atmospheric disturbances of radio reception. However, it was only in 1946 after the Second World War that the first radio source Cyg A was discovered. In 1949 Tau A was identified with an optical object, namely the Crab Nebula.

The peaceful use of V2 rockets was the signal for opening up the atmospheric mantle which surrounds us. The x-ray region of the electromagnetic spectrum was the first such extraterrestrial region to be investigated. In 1948 solar x-ray radiation was discovered by means of films carried outside the Earth's atmosphere by an aerobee rocket. During the next 10 years more precise investigation of solar x-ray radiation disclosed that possible stellar flux lay far below what could be detected at that time. Thus, in 1962 Giacconi et al (Giacconi 62) attempted to measure the fluorescence radiation of the Moon. On this flight, the first extrasolar x-ray source, Sco-X1, the strongest source in the x-ray firmament, was accidentally discovered in the neighborhood of the galactic center. Assuming that the radiation came from a nearby star (approximately 10 parsecs distance), it was necessary to postulate a star with an x-ray luminosity 10^8 times greater than that of the sun--a phenomenon previously unknown and totally unexpected.

*Numbers in margin indicate pagination of foreign text.

Further rocket and balloon flights followed in the next few years. The Moon occultation experiment by Bowyer et al, 1964 (Bowyer 64) is noteworthy since it involved the first successful identification of an x-ray source, again the Crab Nebula.

In 1970, the first x-ray satellite, UHURU, was launched and more than circa 300 cosmic x-ray sources were catalogued. Further satellites were placed in orbit. Today several thousand x-ray sources are known which have the most varied emission mechanisms: remnants of supernovas, pulsars, white dwarfs, neutron stars, quasars, galaxies and possible black holes. Many of them provide us with knowledge about the old age of stars and others instruct us about new aspects of cosmology.

This tumultuous development was further accelerated in recent years by the application of imaging mirror systems. In 1952, H. Wolter described a mirror system which was originally designed for x-ray microscopy. This system consisted of an elongated paraboloid with an attached coaxial and confocal hyperboloid (cf. Figure A.1). In this layout the total external reflection of the x-ray spectrum is exploited even in the case of glancing incidence.

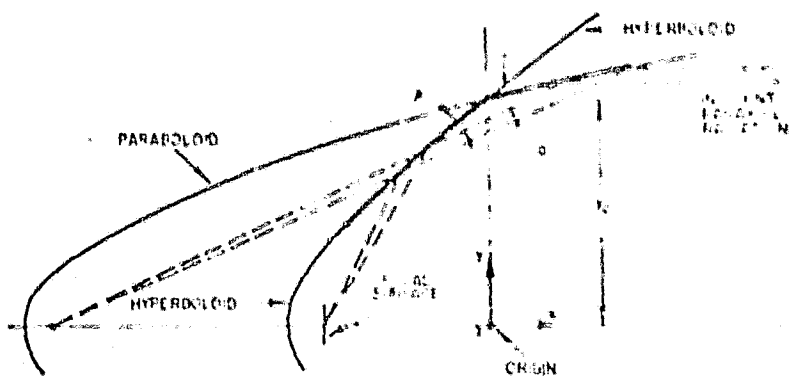

Figure A.1. Mirror telescope after H. Wolter

This technique was adopted for the first time by Giacconi and Rossi in 1960 (Giacconi 60) as the result of their investigation of possible imaging systems for use in x-ray astronomy.

Until 1978, Wolter telescopes were principally employed to /4 study the solar corona on high altitude rockets and, finally, on a skylab mission. However, in the EINSTEIN Observatory (HEAO-B), astronomers now have a mighty instrument at their disposal for investigating the total x-ray sky. It has 10^4 times the sensitivity of UHURU and a resolution of seconds of arc, so that it is competitive with optical telescopes.

In March of last year when the Astro 4/2 payload was launched, the development of a first series of x-ray telescopes at the Max Planck Institute for Extraterrestrial Physics (MPE) was concluded. Three instruments with a diameter of 32 cm were built and tested. One of these telescopes, which was launched with a skylark rocket, transmitted among other things an image of the supernova residue Puppis A. This image was fairly well resolved both spatially as well as spectrally.

Truemper et al (Truemper 79) have described the goal of the present efforts of the MPE x-ray group: to build the biggest x-ray telescope to date, a telescope with an 80 cm aperture, and to launch it by the end of 1984 into Earth orbit on the German x-ray satellite ROBISAT. With substantially better sensitivity and resolution than e. g. UHURU, ROBISAT should carry out a complete survey of the sky, and it is anticipated that some 10^5 new sources will be discovered. Just as in the case of the EINSTEIN Observatory diverse known sources are also to be investigated more closely.

Besides the requirement of good resolving power, above all stringent demands are imposed on the dispersion properties of the telescope. The roughness of the surface in particular is responsible for broad lobes in the point image function which reduce the image contrast. Phenomenonologically, this scattering can be interpreted as the diffraction of x-rays on a statistical grating when the intensity and angular distribution depend on the defining quantities of the grating (e.g., the mean density and the mean grating constant).

In conjunction with the preparations for the 80 cm telescope, /5 the present paper is concerned with the dispersion of wavelength and the angles of incidence as well as with the precise determination of the surface parameters of x-ray mirrors which are extremely well polished. Initially, the paper had two goals: an inquiry concerning the physical nature of x-ray scattering on surfaces, and an effort to improve the technical application of scattering theory. In previous research at this institute (Lenzen 78, Ondrusch 78), the validity of the scalar theory of surface scattering in the wide x-ray region down to circa 5 Å became clear. However, the firm of C. Zeiss improved the technology of manufacturing the x-ray mirrors to the point that the stray flux was hardly distinguishable from the experimental background. Therefore, this paper includes a search for better means of diagnosis. The second goal was the simplification of the iterative process for producing complicated mirror systems. Previously, the quality of a mirror could only be tested adequately in the vacuum test facility of the MPE. As a result, it was necessary to transport a mirror system being tested up to five times back and forth from the point of manufacture to the test site. Such a procedure would be too expensive and risky when constructing the four-fold nested 80 cm telescope. Therefore, the scattering properties of mirrors were also to be investigated for higher energy radiation whose absorption by air is very small. Assuming the validity of the scattering theory, the conclusions reached in work shop testing in the air could then be extrapolated immediately to the x-ray region of interest during actual use.

Besides the above mentioned scalar theory (Beckmann 63) for /6 describing the scattering of x-rays on polished surfaces, based on the so-called physical optics method, there is a vector theory (Rayleigh 07) which takes into account the polarization of the incident and reflected radiation. In Section B, we show that these two theories are equivalent in the special case of interest for this paper, i.e., the case involving slight scattering of x-ray radiation by statistically rough surfaces.

B. The theory of scattering

/7

B.1 The statistically rough surface

This chapter is based on the paper by Church (79a) to which reference is again made later. Figure B.1.1 sketches the scattering of an electromagnetic wave on a rough surface, the coordinate system used and the designation of the angles involved. Suppose that each point (x, y) has a deviation h(x, y) from the mathematical plane such that the xy-plane describes precisely the average plane through the surface:

$$\frac{1}{A}\iint_A h(x,y)\,dx\,dy = \langle h \rangle = 0 \qquad 2.1.1$$

Here A indicates the illuminated surface. The angular brackets define the average over the surface

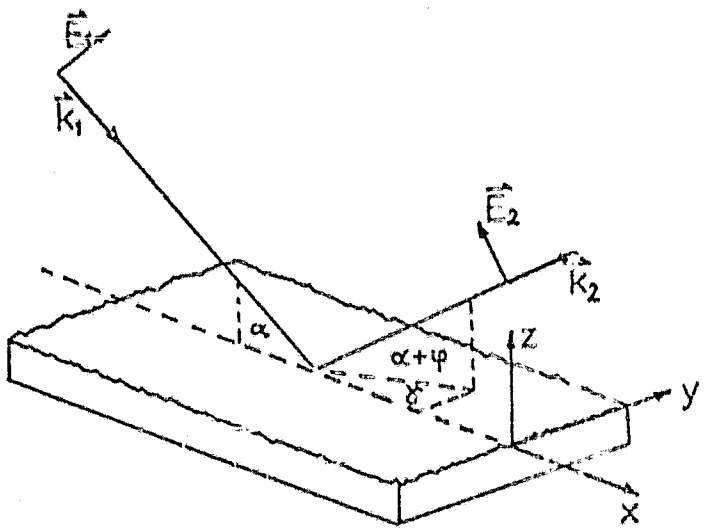

Figure B.1.1: The geometry of scattering on a rough surface

The microroughness σ is defined as the mean square deviation from the ideal plane

$$\sigma^2 = \frac{1}{A}\iint_A h^2(x,y)\,dx\,dy = \langle h^2 \rangle \qquad 2.1.2$$

σ is thus simultaneously the variance of the height distribution $w(z)$. This specifies the relative probability that the height z occurs. The covariance function $B(\tau)$ describes the lateral distribution of the unevennesses on the surface:

$$B(\tau) = \langle h(x_1, y_1) \qquad 2.1.3$$

together with $\tau^2 = (x_1-x_2)^2 + (y_1-y_2)^2$ or its normed equivalent, the autocorrelation function $C(\tau)$:

$$C(\tau) \qquad 2.1.4$$

The correlation length T is the value of τ for which the correla-/8 tion function decreases to the value 1/e.

Let a plane wave $\vec{E}_1$ strike the surface under the incidence angle α and let the wave vector lie in the xz-plane. k_2 describes the propagating wave which is no longer necessarily plane due to scattering. Let γ be the angle between the plane of incidence and the plane of emergence, and let $\alpha + \psi$ be the emergent angle.

For the vector theory which is to be treated later, the different forms of the power spectrum of the surface are also needed. The power spectrum (PSD) is the mean square of the amplitude of the two-dimensional Fourier transform of the surface as a function of the wave numbers p and q:

$$W(p,q) \qquad 2.1.5$$

Thus, the surface is expanded in a Fourier series in the surface wave numbers. The PSD is a measure of how often the frequency combination (p, q) occurs on the surface. $p=2\pi/d_x$ and $q=2\pi/d_y$, where d_x and d_y are the respective surface wavelengths.

There are two special cases of the PSD, one for a one-dimensional rough surface:

$$W_1(p) \qquad \frac{1}{2\pi L}\left| \int_{-L}^{L} e^{-ipx} h(x)dx \right|^2 \qquad 2.1.6 \quad /9$$

and the other for an isotropic surface:

$$W_2(r) \qquad \frac{1}{\pi R^2}\left| \int_{0}^{R} J_0(rx)h(x)dx \right|^2 \qquad 2.1.7$$

where r is the vector sum of p and q: $r^2 = p^2 + q^2$.
J_0 is the null order Bessel function.

The covariance function $B(\tau)$ and the two spectral densities $W_1(p)$ and $W_2(q)$, are second order statistical functions and they are all an expression of the same physical fact. They are interrelated through simple integral transforms. This interrelationship is shown in Figure B.1.2 (Church 79a).

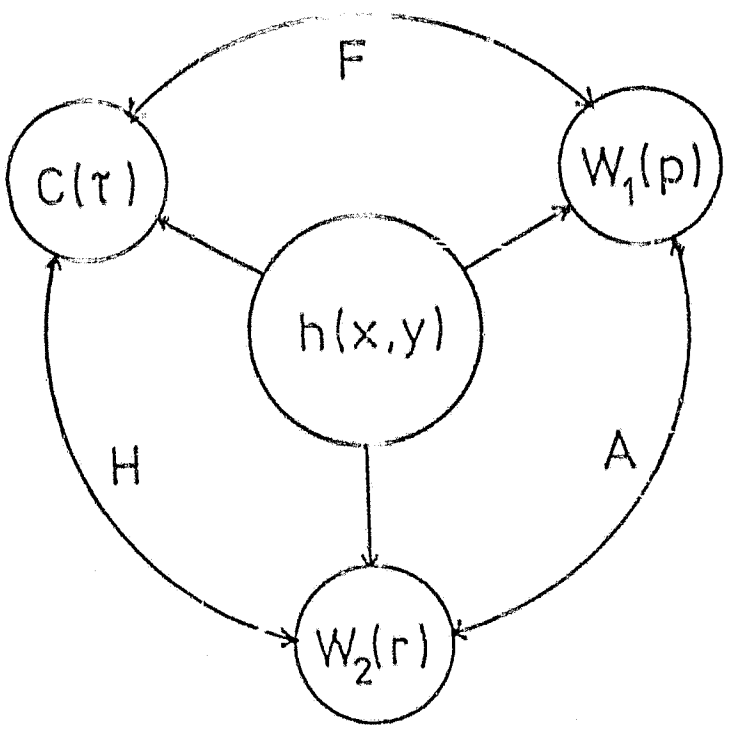

Figure B.1.2: Interrelationship of the statistical functions (Church 79a)

Here the symbols F, H and A on the exterior arrows denote /10
respectively the Fourier, Hankel and Abel transforms. As an example, let us consider the transformation of the covariance function into the two power spectra:

$$W_1(p) = \frac{1}{\pi}\int_0^\infty \cos(p\,\tau)\; B(\tau)\; d\tau \qquad 2.1.8$$

$$W_2(r) = \frac{1}{2\pi}\int_0^\infty J_0(r\,\tau)\; B(\tau)\; d\tau \qquad 2.1.9$$

However, when measuring real surfaces and reducing the data obtained, the simplicity of the conversion between these functions should be taken cum grano salis. It should be remembered that due to cut-off effects and limited resolution, the results can be strangely washed out at times (Church 79a, Church 79b, Elson 69, B.5).

B.2 The scalar theory of surface scattering /11

The scalar theory of the transition of an electromagnetic wave on the boundary surface of two media is based on the Kirchhoff approximation to the boundary conditions for the Helmholtz integral--the so-called method of physical optics. At each point P of the separation surface, the electromagnetic field is approximated by the field on the associated tangent plane. This approximation is valid provided that the radius of curvature at P is large compared to the wavelength of the incident radiation:

$$4\,\pi\, r_c \sin\alpha \gg \lambda \qquad 2.2.1$$

This method has been applied repeatedly in all details to statistically rough surfaces (Beckmann 63, Lenzen 78, Carniglia 79). Therefore, following Beckmann's formulation, I shall present here only the salient results.

To begin with, some definitions:
Let the momentum transfer from $\vec{k}_1$ to $\vec{k}_2$ be $\vec{v}=\vec{k}_1 - \vec{k}_2$:

$$v_x = k(\cos(\alpha+\varphi)\cos\gamma - \cos\alpha)$$
$$v_y = k\cdot\cos(\alpha+\varphi)\sin\gamma)$$
$$v_z = k(\sin\alpha + \sin(\alpha+\varphi))$$
$$v_{xy}^2 = v_x^2 + v_y^2 \qquad 2.2.2$$

A projection factor F derived by Beckmann is given by

$$F = \frac{1 + \sin\alpha\sin(\alpha+\varphi) - \cos\alpha\cos(\alpha+\varphi)\cos\gamma}{\sin\alpha\,(\sin\alpha + \sin(\alpha+\varphi))} \qquad 2.2.3$$

The factor which essentially determines the scattering constituent is:

$$q = \sigma^2 v_z^2 = (k\ (\sin\alpha + \quad\quad))^2 \qquad 2.2.4$$ /12

Next, Beckmann assumes that the altitudes are normally distributed:

$$w(z) = \frac{1}{\sqrt{2\pi}\,\sigma}\ e^{-(\quad)^2/\quad} \qquad 2.2.5$$

From equations 6, Chapter 5.2, and 32, Chapter 5.3 of his paper, we obtain the following equation for the point image function of the mirror:

$$\frac{1}{I_r}\left(\frac{dI}{d\omega}\right) = e^{-q}\left[\ \delta(\varphi,\gamma) + \frac{\quad}{A}\sum_{n=1}^{\quad}\frac{\quad^n}{n!}\int_0^{\quad} J_0(\quad v_{xy}\ t\ \quad)\ \quad\ \quad\ \quad\ \right] \qquad 2.2.6$$

Here I_r is the total reflected intensity, $d\omega$ the solid angle element $\cos(\alpha+\psi)\,d(\alpha+\psi)\,d\gamma$ and A is the coherent illuminated surface. The remaining quantities have already been defined in the preceding part.

In relation to the total reflected intensity, the intensity derived from Equation 2.2.6 and scattered into a solid angle element, is made up of two parts. The first term on the right side is the coherent part reflected in the specular direction ($\psi=\gamma=0$). The second part, which is henceforth called the dispersion halo, furnishes the intensity of the radiation scattered in the given direction.

Next, let us discuss the specular direction. The total specular reflected intensity is

$$I_{spec} = \quad 2.2.7$$

where

$$g_o = \quad 2.2.8$$

This extremely important result, which is similar to the Rayleigh criterion, can also be obtained by means of other formulations (B.3). As early as 1961, it was applied to surfaces of optical quality (Bennet 61). It provides a simple method for determining the micro roughness of a surface:

$$\sigma = \sqrt{-\ln (I_{spec} / I_r)} / 2k\sin\alpha \qquad 2.2.9 \qquad /13$$

The second term of the right side of 2.2.6, the dispersion halo, is still somewhat unclear. However, the integral over the Bessel function can be calculated for every given autocorrelation function. In D.4, this is carried out for several examples.

For the special case of small scattering ($g_o \ll 1$) the sum over m can be broken off after the first term with the following result:

$$\frac{1}{I_r}\left(\frac{dI}{d\omega}\right)_{scat} = \frac{2\pi F^2 g}{A\,\sigma^2} \int_0^\infty J_0(v_{xy}\tau)\, B(\tau)\, \tau\, d\tau \qquad 2.2.10$$

The integral over the Bessel function is the Hankel transform of the covariance function and is known from B.1 as the isotropic PSD $W_2(v_{xy})$. For grazing incidence ($\alpha \ll 1$) g becomes equal to $g = g_o F^2$. In this case, we have a simple expression for the dispersion halo

$$\frac{1}{I_r}\left(\frac{dI}{d\omega}\right)_{scat} = \frac{16\pi^2 k^2}{A}\,\alpha^2 \quad W_2(v_{xy})\, F^4 \qquad 2.2.11$$

Thus, the special case of small scattering distribution merely reproduces the power spectrum of the surface evaluated for the local wavelength given by $d = 2\pi / v_{xy}$. The leading factors are purely geometric factors by means of which the form of the factor

given in 2.2.3 is discussed in the literature (Garcia 79, Hill 78, Garibaldi 75).

Besides the criterion 2.2.1 which restricts the validity of the Kirchhoff approximation to large radii of curvature, Beckmann introduces some further simplifications:

1. Assume that the change in the gradient of the surface is so small that the Fresnel reflection coefficient for the microscopic angle of incidence, namely ϑ , $R(\vartheta)$ can be replaced by $R(\alpha)$, the coefficient for the macroscopic angle of incidence.

2. Shading effects and multiple scattering are neglected. /14

3. Let the incident wave be plane and linearly polarized. Let the E vector lie in the plane of incidence.

4. Only the remote radiation field is considered, i.e., assume that the point of observation is so far from the surface that the scattered waves can be considered as plane waves.

B.3 The first order vector theory of pertubation /15

The scalar theory of surface scattering treated in the last section is valid over a wide domain of surface roughness and wavelengths. Thus, e.g., the scattering of radio waves on the Earth and the Moon can be described just as well as the scattering of x-rays on polished surfaces. In this connection, pure scattering is defined by the mechanism in 2.2.7. For small scattering ($k\sigma << 1$) there results a quadratic dependence of scattering on the product of roughness, wave number and incidence angle with $I_{scat}/I_r = \sigma_o$

For x-ray scattering on highly polished surfaces, only the case of a relatively smooth surface and a consequent slight amount of scattering is interesting. Here some of the approximations built into the Beckmann theory are unnecessary and a precise vector

formalism can be derived. In contrast to the scalar theory, the vector theory considers the polarization states of the incident and emergent radiation.

In the smooth surface limit, the intensity dispersed into the solid angle element $d\omega$ in the direction (ψ,γ) in relation to the total incident intensity I_i is given by

$$\frac{1}{I_i}\left(\frac{dI}{d\omega}\right)_{scat} = 4\ k^4\ \sin\alpha \sin^2(\alpha+\varphi)\ \ Q\ \ W(v_x,v_y) \qquad 2.3.1$$

This equation represents the first term of the expansion of the scattering in terms of the quantity $(k\ \sigma)^2$ according to the vector perturbation theory and is a generalization of the original result obtained by Rayleigh (Rayleigh 07, Barrick 70). It decomposes into factors which illustrate the physics incorporated: K^4 is the so-called Rayleigh blue-sky factor, the angle functions are projection factors, Q is dependent on material and polarization properties only and W is the power spectrum of the surface which is known from 2.1.5, evaluated for the surface wave numbers given by 2.2.2. The total dependence of the scattering on the topology/16 of the surface is thus concealed in the surface factor $W(v_x, v_y)$. In the case of scattering on a statistically rough surface, $W(v_x, v_y)$ can be replaced by $W_2(v_{xy})$, the isotropic power spectrum (cf. 2.1.7).

In general, Q is a complicated function of the incident and emergent angles, the incident and emergent polarization states and the complex indices of refraction of the separation surface. However, in the limiting case of glancing incidence, Q converts into the Fresnel reflection coefficient $R(\alpha)$. A comparison with the total reflected intensity yields a simpler form of 2.3.1:

$$\frac{1}{I_r}\left(\frac{dI}{d\omega}\right)_{scat} = 4\ k^4\ \alpha\ (\alpha+\varphi)^2\ W_2(v_{xy}) \qquad 2.3.2$$

Next, let us introduce a leading factor F_c corresponding to 2.2.3:

$$F_c = 1 + \varphi/\alpha \qquad 2.3.3$$

Then we obtain:

$$\frac{1}{I_r}\left(\frac{dI}{d\omega}\right)_{scat} = 4\, k^4\, \alpha^3\, W_2(v_{xy})\, F_c^2 \qquad 2.3.4$$

In order to obtain the integral dispersion component, we must integrate 2.3.4 over $d\omega$:

$$S = \frac{1}{I_r}\int_0^{4\pi}\left(\frac{dI}{d\omega}\right)_{scat} d\omega = \frac{I_{scat}}{I_r} \qquad 2.3.5$$

This is possible in the case of a small scattering angle (F_c=1). From 2.1.7 we obtain:

$$\int_0^{4\pi} W_2(v_{xy})\, d\omega = \frac{\sigma^2}{\alpha k^2} \qquad 2.3.6$$

Hence

$$S = 4\, k^4\, \alpha^3\, \frac{\sigma^2}{k^2} = g_o \qquad 2.3.7$$

This is the integral criterion which corresponds to 2.2.8. In the original Beckmann theory, a normal distribution of heights was assumed; here the result is obtained without any such distribution assumption. However, it is easy to show that in the limiting case of the scalar theory for small roughnesses, the integral statements are likewise independent of the height distribution of the surface.

A comparison of the angular distribution of the scattering according to the vector theory (2.3.4) with the result obtained from the scalar theory (2.2.11) shows an extensive agreement:

In both cases, the dependence of scattering on the topology of the surface is described by the isotropic power spectrum density $W_2(v_{xy})$.

The Beckmann asymmetry factor F can be developed into $F=1+\psi/2\alpha$ for ($\alpha,\psi \ll 1$). Hence, $F^4 = F_c^2$ up to the second order of ψ/α.

From a comparison of the leading factors, we obtain an expression for the normalizing factor A, which is somewhat non-intuitive in the Beckmann theory: /17

$$A = \frac{\lambda^2}{\alpha} \qquad 2.3.8$$

Both the differential and integral statements of the two theories concerning the scattering of x-rays on statistically rough surfaces agree in the limiting case of small roughnesses and small scattering angles. For large scattering angles, the two statements still agree up to the second order of ψ/α.

B.4 Summary of the scattering theory /18

Here in summary fashion we shall present again the most important equations used. From the scattering component, the micro roughness can be determined as:

$$\sigma = \frac{\sqrt{S}}{2k\alpha} \qquad 2.4.1$$

The point image function of the mirror is:

$$\frac{1}{I_r}\left(\frac{dI}{d\omega}\right) = (1-q_o)\ \delta(\varphi,\gamma) + 4k^4\alpha^3 W_2(\nu_x) F_e^2 \qquad 2.4.2$$

The split image function is the point image function integrated over γ and it contains the one-dimensional power spectrum:

$$\frac{1}{I_r}\left(\frac{dI}{d\varphi}\right) = (1-q_o)\ \delta(\varphi) + 4k^3\alpha^3 W_1(\nu) F_e^2 \qquad 2.4.3$$

For later application, we shall now calculate some examples of power spectra from their covariance functions. Because of their mathematical simplicity, we shall consider the following two covariance functions:

$$B(\tau)_1 = \sigma^2 \exp - (|\tau|/T) \quad \text{exponential} \qquad 2.4.4$$

$$B(\tau)_2 = \sigma^2 \exp - (\tau/T)^2 \quad \text{Gaussian} \qquad 2.4.5$$

From 2.1.8, we obtain:

$$W_1(\nu)_1 = \frac{1}{\pi}\frac{\sigma^2 T}{1+(T\nu)^2} \qquad 2.4.6$$

$$W_1(v)_2 = \frac{1}{2\sqrt{\pi}} \sigma^2 T \exp - (Tv/2)^2 \qquad 2.4.7$$

where $v = v_x(\alpha, \gamma = 0) = k \cdot \ldots = k \cdot \sin(\alpha + \varphi/2)$

Analogously from 2.1.9: /19

$$W_2(v_{xy})_1 = \frac{1}{2\pi} \frac{\sigma^2 \quad T}{(1+(Tv_{xy})^2)^{3/2}} \qquad 2.4.8$$

$$W_2(v_{xy})_2 = \frac{1}{4\pi} \sigma^2 T^2 \exp - (Tv_{xy}/2)^2 \qquad 2.4.9$$

B.5 The normal distribution of heights and the exponential autocorrelation

In treating statistically rough surfaces, it was assumed in Chapter B.2 that the heights were normally distributed. By measuring surfaces with optical quality, Eastman et al (Eastman 74) and /20 Elson (Elson 79) obtained the best fit with an exponential autocorrelation function, in comformity with Lenzen's results (Lenzen 78). To test these assumptions, a bad sample (rms roughness circa 170 Å) was measured with the Perthometer. Here the point of the stylus instrument had a diameter of 1 µm and the measurement range was circa 2 mm. Figure B.5.1 shows the profile of the measured heights and the resulting height distribution.

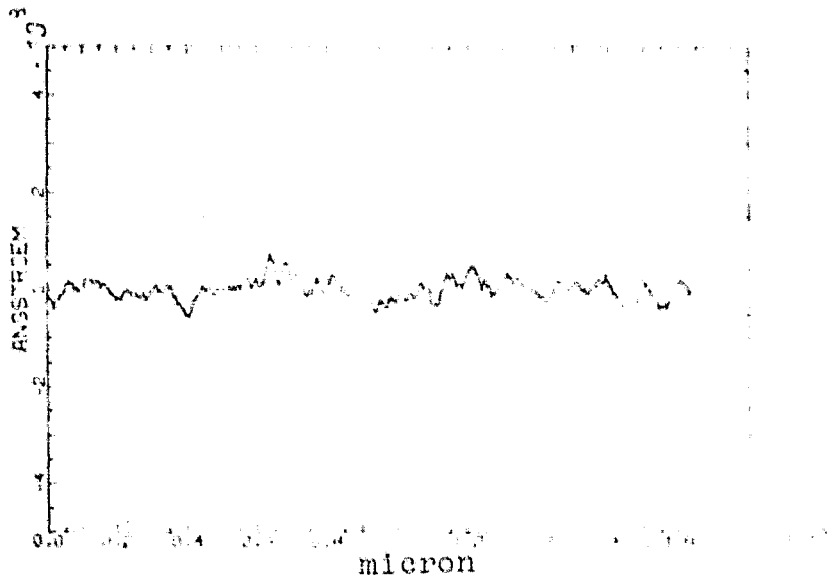

Figure B.5.1: The sufrace profile measured with the Perthometer

A good approximation to the distribution of heights can be obtained by means of a Gaussian function with a variance of circa 170 Å. The autocorrelation calculated according to 2.1.3 exhibits a period corresponding to approximately half the measurement range and a shortwave period of circa 50 µm. These effects could be the result of the imperfection of the sample referred to in B.1. For this reason, statements about the autocorrelation function are meaningful only in the region $\tau<50$ µm. Figure B.6.4 shows $C(\tau)$ /21 in the region up to 100 µm . Between 0 and 50 µm a Gaussian curve with $T_g = 25$ and an exponential curve with $T_e = 30$ µm were fitted. As the figure shows, $C(\tau)$ is more closely approximated by the exponential curve.

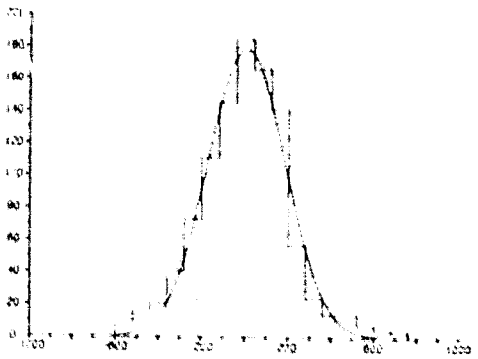

Figure B.5.2: Distribution of heights

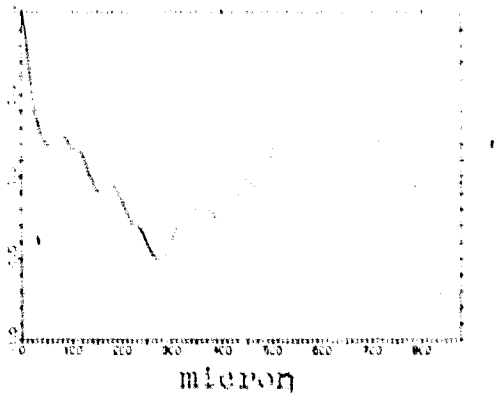

Figure B.5.3: The autocorrelation function

In Chapter D.4, further comparisons of different autocorrelation functions were made. These also turn out in favor of an exponential curve.

C. Measurements on samples of plane mirrors

C.1 Description of the measurement procedure

The measurements of x-ray scattering were carried out at the two test installations of the MPE, PANTER and ZETA. These facilities

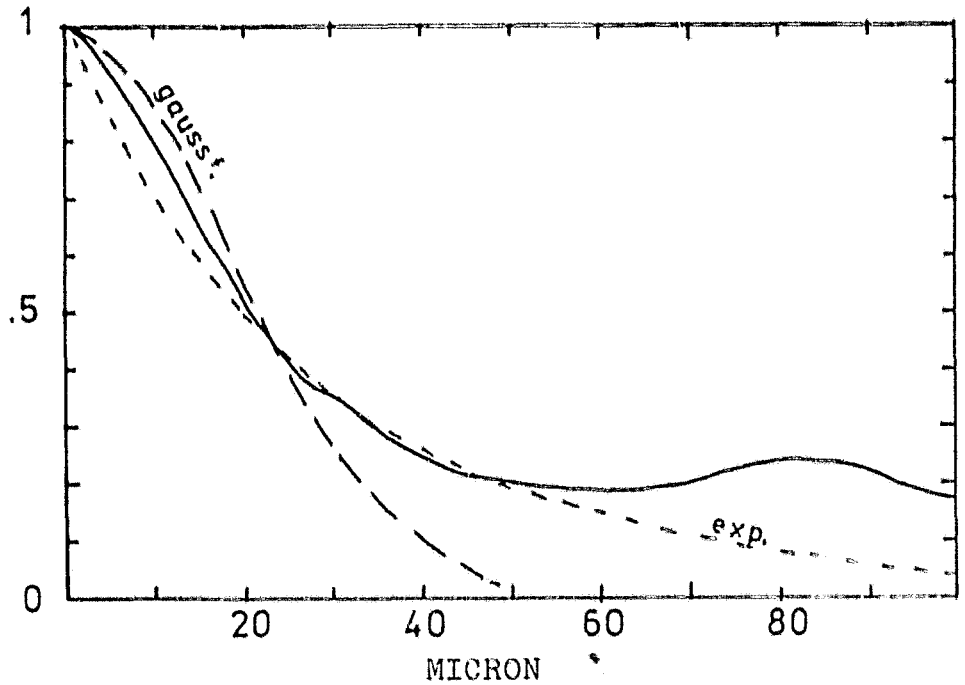

Figure B.5.4: The autocorrelation function for small correlation lengths.

have been described by Aschenbach et al (Aschenbach 79). The general measurement assembly is shown in Figure C.1.1.

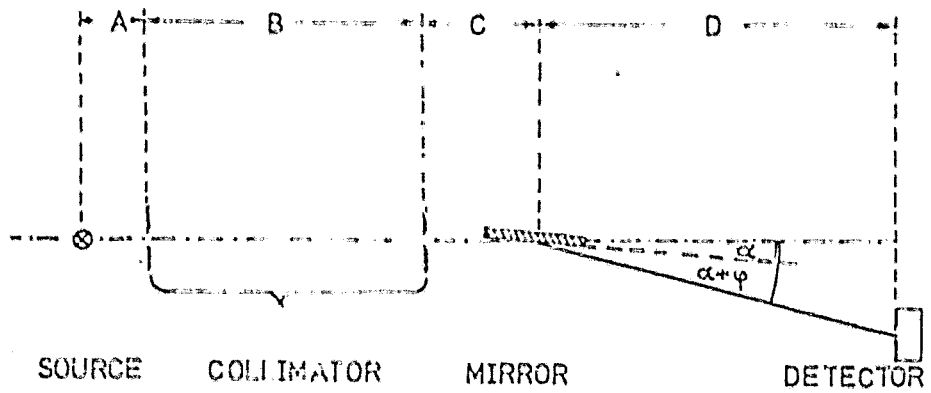

/22

Figure C.1.1: Layout of the measurement apparatus

A focusing source generates a characteristic spectrum of soft x-rays. By means of two slits, one of which is 0.15x20 mm^2, and the other 0.10x10 mm^2, a beam with divergence of five and 10 seconds of arc is reflected on the sample mirror so that the field is cut down. At a distance of about 3.4 m from the mirror, the dispersion distribution is begun with a proportional counter tube having a

0.10x10 mm^2 entrance slit and is compared with the profile of the direct beam. Since soft x-rays are absorbed in air, it is necessary to make the measurements at a pressure of circa 10^{-5} mm Hg.

The adjustment of the equipment and the mirror is as follows:

The optical axis of the equipment is defined by two laser beams which are incident on each other. The collimeter slit is measured by their diffraction patterns and lined up. The parallelism of the slit is ensured by the diffraction patterns which are placed horizontally. The laser beam which is reflected by the mirror must /23
also lie in the plane defined by the optical axis and the diffraction patterns. The manipulator which provides for the turning of the mirror about the z-axis was calibrated by means of the laser. By means of the x-ray beam, the mirror is placed parallel to the optical axis in a vacuum. It is then moved into the path of the rays until it shades half of the intensity. Next, the mirror is turned about the z-axis until the intensity is a maximum. The desired grazing angle is set with respect to the zero setting thus defined; then the mirror is again placed in the middle of the direct beam and from there is moved approximately half the projected length of the mirror. Then the counter tube is used to determine the maximum intensity of the direct beam. The beginning of the scattering distribution in the plane of the detector is regulated by means of an HP 9830 processing computer. A dynamic measuring procedure is used here in which the integration time in each case and the density of the measurement points for the anticipated distribution are matched. The duration of a measurement is approximately two hours. Figure C.1.2 provides an example of the measurement of a scattering distribution. The break down of the measurement range ($\pm \varphi_o$) and the density of the measured points together with the integration time in each case are shown in Table I.

Normally, the maximum scattering angle measured 20', and in the case of the sample 38A, 60' (cf. C.2).

range	Halo S_-	specular Region	Halo S_+
grazing angle	$-\varphi_0 \leq \varphi \leq -2'$	$-2' < \varphi < 2'$	$2' \leq \varphi \leq \varphi_0$
density of the measured points	3 points/ arcmin	42 points/ arcmin	3 points/ arcmin
integration time	40 sec	5 sec	40 sec

Table I. Definition of the measurement range

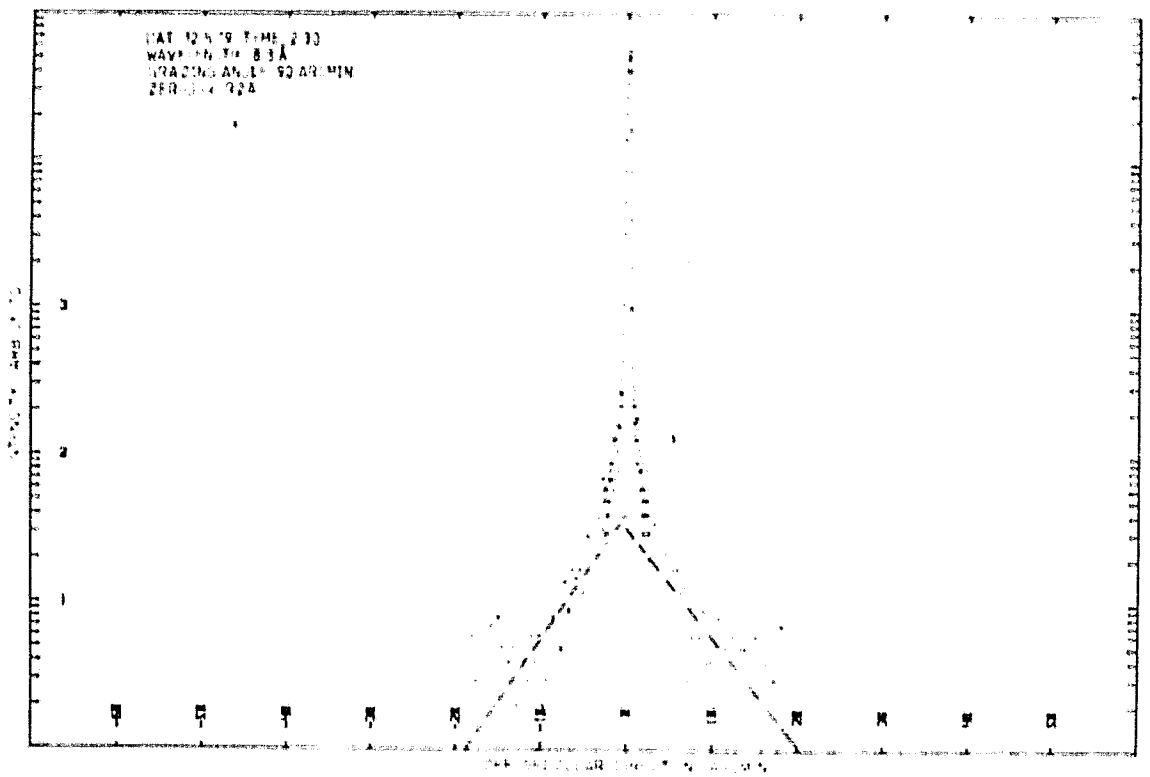

Figure C.1.2: Example of an original measurement curve

The measurement data were evaluated on the one hand in an online computer (raw data evaluation), and on the other hand, they were recorded on tape and later evaluated at the IBM computer installation (cf. D.3). To evaluate the raw data exponential functions were fitted to the measurement points in S_+ and S_-; then the total scattering intensity was treated as the sum of six terms:

$$I_{scat} = S1 + S2 + S3 + S4 + S5 + S6 \qquad 3.1.1$$

S1: the extrapolation from $-\alpha$ to $-\psi_o$
S2: the integral over the measurement points in S_-
S3: the extrapolation from -2 to 0 minutes of arc
S4: the extrapolation from 0 to 2 minutes of arc
S5: the integral over the measurement points in S_+
S6: the extrapolation from ψ_o to $+\infty$

The integral scattering component was:

$$S = I_{scat} / I_r \qquad 3.1.2$$

Here the total reflected intensity I_r was the integral over the entire set of measurement points plus the extrapolations S1 and S6. All terms were corrected for a background of 0.05 counts/sec in the case of PANTER, and 0.02 counts/sec in the case of ZETA. The surface roughness was then determined by Equation 2.4.1. /25

C.2 Tie-in with earlier measurements /26

In order to link up with the earlier measurements made by Lenzen (Lenzen 78), a sample which he measured (38A) was again extensively investigated. Sample 38A is a gold-deposited Kanigen mirror, 100 mm in diameter with roughness of circa 100 Å and a correlation length of circa 10 µm. Since small angles of incidence are necessary in the case of the high energies applied later, we investigated angles down to 15 minutes of arc. In this range, special effects were expected (shadings, multiple reflections). In Table II, these measurements are compared with Lenzen's results.

TABLE II: Comparison with previous measurements

angle (arcmin)	15	20	30	45	60	15	20	30	45	15	20
wavelength (Å)	13	13	13	13	13	8	8	8	8	8	8
σ_{Lenzen} (Å)			111	102	98			96	91		
$\sigma_{Hasinger}$ (Å)	135	125	118	100	97	111	107	100	98	92	90

There is good agreement. In the case of small incidence angles, the results are of a somewhat higher order, but are not out of proportion, however. Even a change in the surface over time cannot be regarded as significant.

C.3 Extremely well-polished zerodur samples /27

TABLE III. Summary of the measured zerodur samples

sample	vapor deposit	size	measurements	facility
Ronde 1 Zerodur	-	200mm Ø	9	PANTER
Ronde 2 "	-	200mm Ø	6	"
Ronde 3 "	-	220mm Ø	13	ZETA
R1A "	Nickel	165x32mm	15	PANTER
R1B "	"	101x32mm	3	"
R2A "	platinum	165x32mm	15	"
R2B "	"	101x32mm	3	"
R3A "	Gold	165x32mm	15	"
R3B "	"	101x32mm	14	"
R4A "	-	165x32mm	12	ZETA
R4B "	-	101x32mm	-	-
A "	Gold	100mm Ø	14 20	PANTER ZETA
B2 "	Gold	100mm Ø	15	ZETA

Within the scope of the AXAF[1] program for testing mirror materials and polishes and also in conjunction with the 80 cm telescope, the firm of C. Zeiss, Oberkochen, manufactured plane mirrors of very good quality with various kinds of surface finishes. For this purpose, two zerodur disks were made first of all. They were investigated in the MPE (disk 1, disk 2). Cut into rectangular bars and with deposits of various materials, they were again returned for subsequent testing in PANTER. Two gold covered zerodur mirrors

[1] Advanced x-ray astrophysics facility

manufactured earlier (A and B2) as well as an additional disk were measured. In Table III, the samples, materials and the number of scattering measurements at the respective test facilities are tabulated.

An objective of this work was to check the assertions of the /28
scattering theory in the higher energy range also so as to make possible a subsequent shop test of the telescope in the air. The energies necessary for this purpose range between 6 and 10 keV, and the resulting critical angles are in the neighborhood of 15 minutes of arc. The highest photon energies to be followed up were 4.5 keV in the case of PANTER and 6.5 keV in the case of ZETA. In order to obtain comparable statements, the following characteristic lines were chosen:

Cu - L	13.3 Å	0.9 keV
Al - K	8.3 Å	1.5 keV
Ti - K	2.8 Å	4.5 keV
Fe - K	1.9 Å	6.5 keV

Incident angles between 10 and 150 minutes of arc were measured.

In the evaluation of raw data, essentially two effects appeared:

For these extremely good samples and the chosen geometry, the scattering distribution lies about four powers of 10 below the specular maximum (cf. Figure C.1.1). However, in this range the direct beam has a comparable halo (cf. D.1). But the measured scattering intensity for some curves is lower than the comparable intensity in the direct beam. As is shown explicitly in Chapter D.2, this effect can be understood as a masking of the direct beam by the mirror. If we plot the microroughness obtained by the process described in C.1 against the ratio of the incidence angle to the wavelength, (which I shall henceforth call the "diffraction number"), then we obtain not a constant, as might be expected, but a kind of hyperbola with a finite asymptote about which the measurement values are more or less scattered. Figure C.3.1 shows this curve for the example of the sample R2A.

The roughness measured for large diffraction numbers is somewhat constant, while the roughness measured for small diffraction numbers rises disproportionately high. This effect will be illuminated in D.5 from still another side.

/29

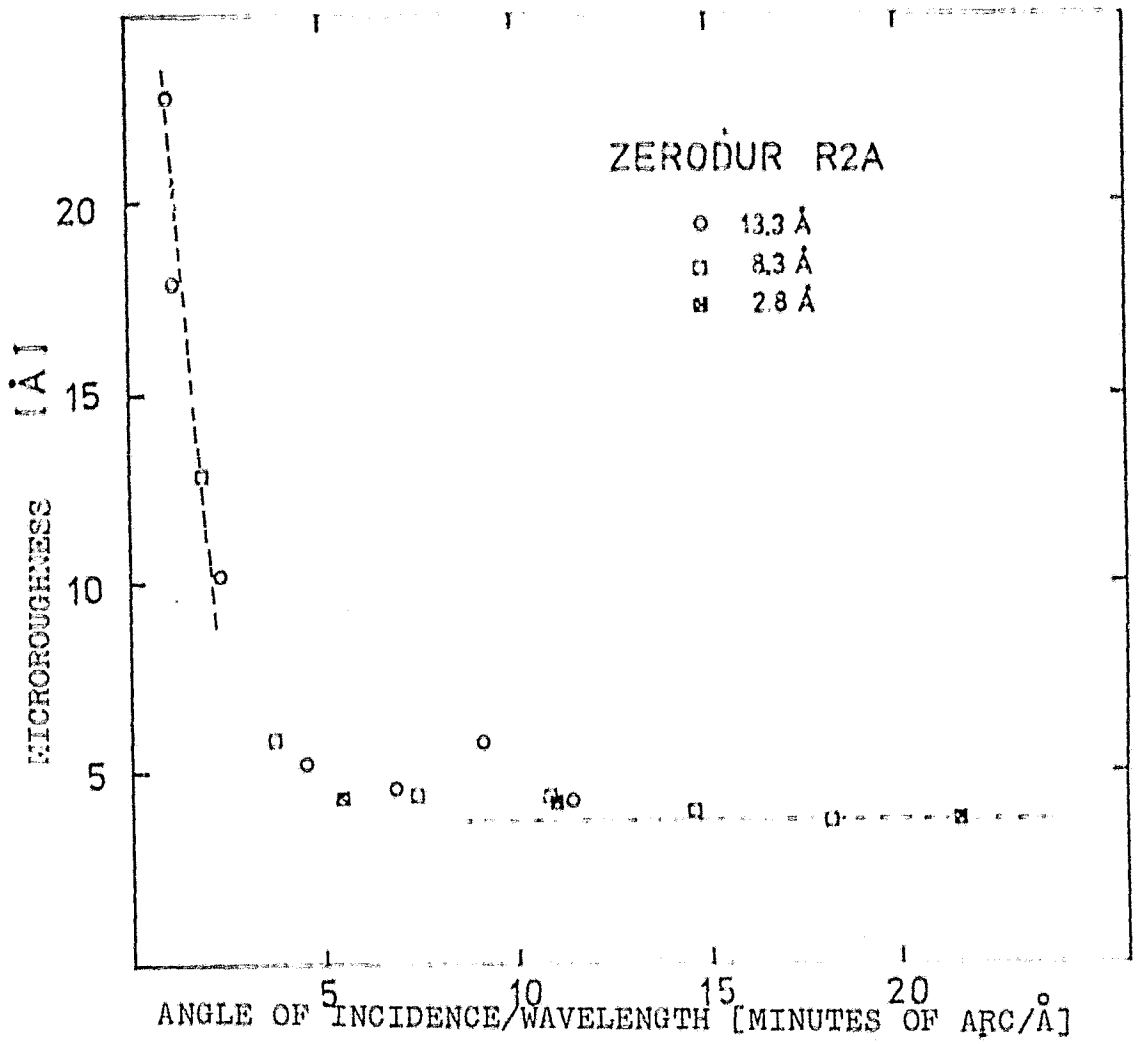

Figure C.3.1: Measured roughness of the sample R2A

Probe	λ [Å] / α [']	13.3									8.3									2.8						2.4	1.9		
		15	20	30	45	60	75	90	120	150	15	20	30	45	60	75	90	120	150	10	15	20	30	45	60	15	5	10	15
38A		135	125	118	97						114	107	101	98	X						92									
Sonde 1	U												2.4		2.2		1.6					3.2								
	O												2.4		2.4		1.6					2.1	3.6							
Sonde 2	U												5.3		3.4		5.1					2.8	4.7							
	O														3.9															
Zerodur A	M														4.7			4.4	5.0										
(Panter)	O		18.4	12.6		5.8			5.3	5.1					4.7			5.0	4.9				5.6		5.5				
Zerodur A	M	37.4		18.9		7.0		5.0			29.5		12.4		5.5		5.1				5.9		3.9	4.6						
(ZETA)	O	44.1		18.9		7.8		5.3			31.6		12.4		5.0						4.9		4.2	4.2						
11A		19.7		7.9		3.6		3.3	2.8	2.6	12.2		3.3		3.3		3.3	2.9	X		2.4		2.0		X					
11B				9.9		4.3		4.8																						
12A		22.9		10.3		5.3		4.7	5.9	4.3	12.9		5.9		4.5		4.2	4.0	3.7		4.4		4.2		3.8					
12B		21.7		10.9				4.7																						
13A		17.9		7.6		4.3		4.3	3.5	2.9	11.7		4.5		4.0		3.3	2.9	2.6		1.1		1.7		2.6					
13B				4.9		2.6		2.9	2.9	2.9	9.2		3.0		2.4		2.8	2.5	2.9		2.7		2.5		2.5					
32		16.3		7.4		4.0		3.2			10.7		5.4		3.4		2.4				3.2		3.5	2.9	2.7	3.0	3.2	2.6	2.5	
14A		20.7	15.4	10.2							11.2		5.9		4.1					3.6	2.8		2.8				4.2	1.5	1.1	
Sonde 3	A	78.0	59.3					8.1	5.1	4.8	35.7		13.5		3.4	3.9					3.6		1.8							
			40.1					7.5							7.2															

TABLE IV: The measurement program and the results of the evaluation of raw data.

In Table IV, the computed surface roughness is tabulated for all the measurements. An important result is the fact that the scattering quota obey the surface scattering theory both in the case of low energies (0.9-1.5 keV), as well as in the case of high energies (4.5-6.5 keV) provided that the diffraction number exceeds circa five minutes of arc/Å. Thus, the microroughness measured in /31
the air at a shop would be comparable to the roughness occurring in the subsequence range of application.

C.4 Improvement of the test assembly /32

The experience gained in the first measurement series at the PANTER facility was put to use in improving the test assembly in the further measurements at the ZETA facility following the dismantling of PANTER. In making the measurements, the essential sources of error were the following, besides those described in D.3:

1. The stability of the primary flux from the x-ray source:
   The intensity and possibly also the distribution of the directions of the x-ray emission varied due to a change in the pressure in the x-ray tube, to contamination of the anticathode and instabilities in the voltage supply.
2. The mechanical stability
   The adjustment of the test assembly is extremely sensitive to shocks. Even any wandering of the focus on the anticathode can cause changes in the intensity of the collimated direct beam.
3. Stray light in the facility.
   It turns out that stray light which is probably reflected over the beam tube walls flickers about in the facility. Its intensity lies somewhere in the neighborhood of the expected stray halo.
4. Beam interception by the mirror.
   The projection surface of the mirror acts as a slit which has a different opening for each angle of incidence (cf. C.2, D.3). This leads to uncertainties when the direct beam is considered later. Since the halo intensity of the direct and the reflected beam is approximately equal, it is of decisive importance, where

and how the direct beam is cut off. Both cannot be uniquely determined by the measurements.

The errors described were substantially rectified as follows: Figure C.4.1 shows the general test assembly and the newly mounted components.

/33

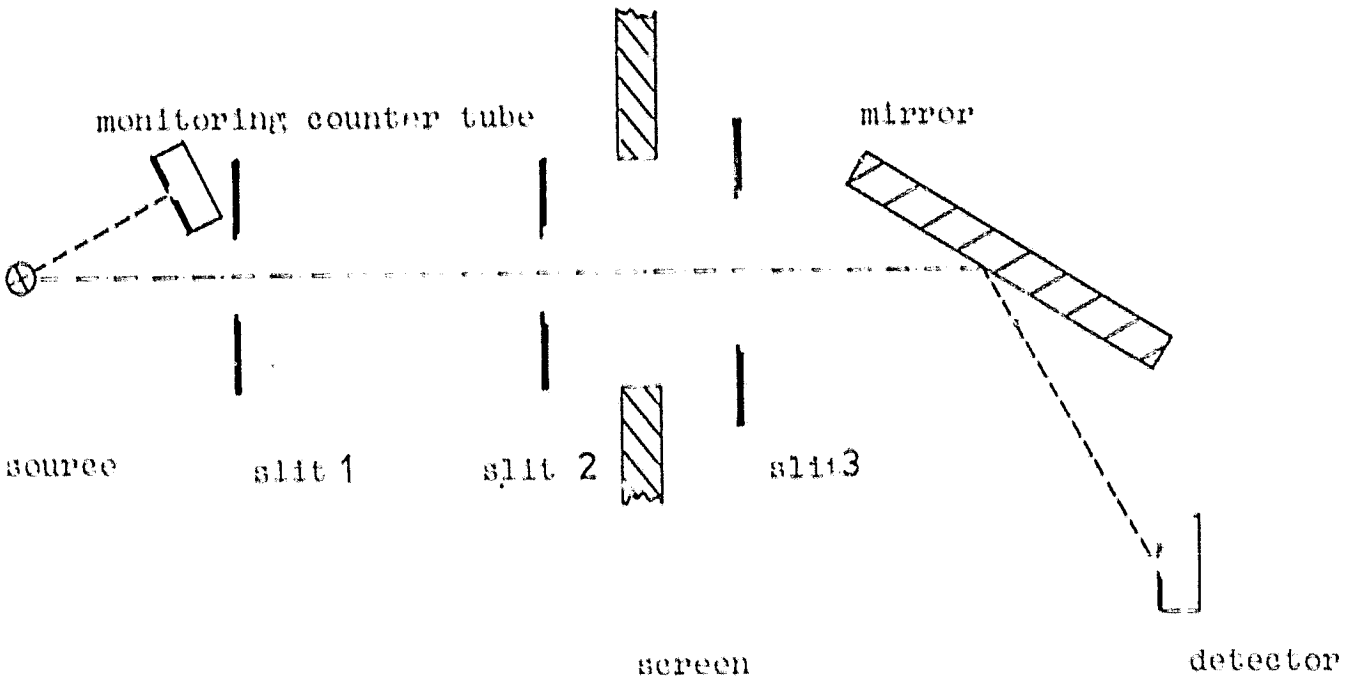

Figure C.4.1: Improvement of the measurement setup

Re 1:
A monitor counter tube was mounted in the x-ray tube near the source. Its opening is so designed that the registered intensity corresponds approximately to that of the test counter tube in the direct beam. Thus, variations in the intensity of the source and in the spectrum can be controlled. It turned out that normally the variations were not substantially greater than 10% per day. In unfavorable cases, principally due to contamination, the source spectrum varied markedly (circa 30%).

Re 2: /34

The errors mentioned here are purely statistical in nature and can hardly be eliminated. However, it turned out that measurements made at night and after longer periods of continucus operation give rise to the least complications.

Re 3:

The beam tube was completely walled off by a large aluminum screen between slit 2 and the mirror. Only one opening of about 50 mm remained free for the passage of the beam.

Re 4:

In order to obtain a measurable beam geometry, independent of the angle of incidence, a third slit, 0.8 mm wide, was mounted close in front of the mirror. The profile of the direct beam is now defined in the halo by this aperture. Diffraction on this slit can be neglected. As long as the projected mirror surface is broader than 0.8 mm, the direct beam and the specular direction of the scattering distribution are equivalent.

After these corrections were made at the ZETA facility, the incidence-angle dependent microroughness effect occurred again. Hence, the cause is clearly not to be found in the mirrors mentioned here.

D. Evaluation and results /35

D.1 The direct beam

The direct beam displays extensive lobes near circa 10^{-4} times the central intensity. This effect is relatively independent of the wavelength. To begin with, an attempt was made to explain this profile as a consequence of diffraction at the collimator slit. Figure D.1.1 is a sketch of the geometry of the simplified model which was assumed for this purpose.

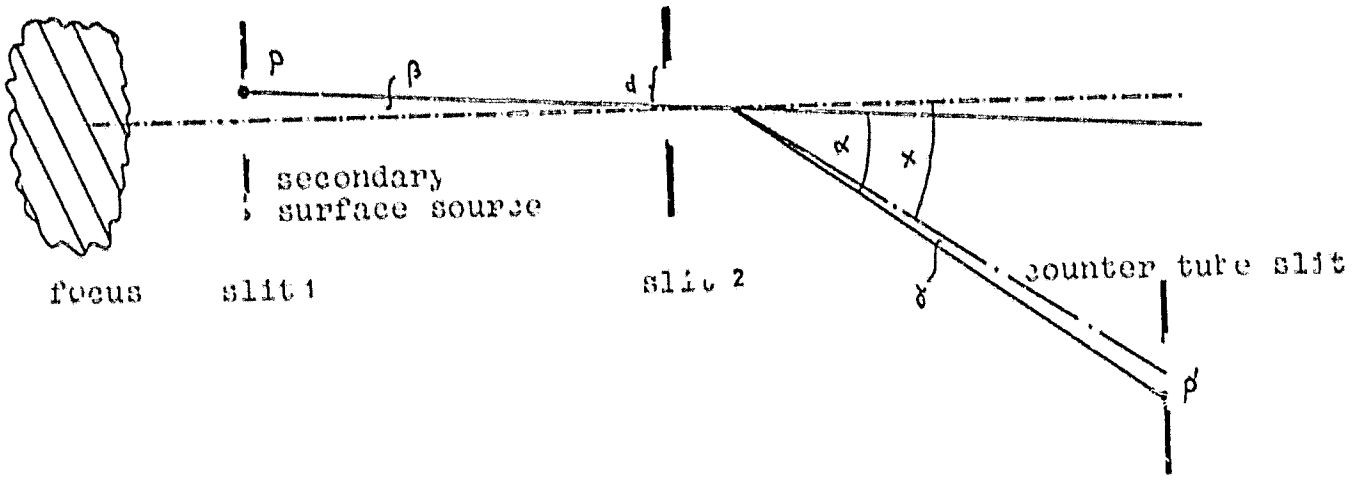

Figure D.1.1: Geometry of the simplified model for calculating the profile of the direct beam

$$\alpha = x + \beta + \gamma \qquad 4.1.1$$

The origin is a homogeneously radiant surface source such that the slit 1 can be assumed to be a secondary surface source. Let P be a point source from the continuum in slit 1. Suppose that the distance to slit 2 is large enough so that the wave fronts can be regarded as plane here, i.e., it is sufficient to apply the Fraunhofer refraction analysis in this instance. The intensity at a point P' behind the second slit is:

$$D(\alpha) = \frac{\sin^2(2\pi Q\alpha)}{(2\pi Q\alpha)^2} \qquad 4.1.2$$

/36

where $\alpha \ll 1$, $Q = d/\lambda$. From 4.1.1, it follows that

$$D(x, \beta, \gamma) = \frac{\sin^2(2\pi Q(x+\beta+\gamma))}{(2\pi Q(x+\beta+\gamma))^2} \qquad 4.1.3$$

To obtain it from the intensity due to the surface source, it is sufficient to integrate over β, since the source may be regarded as incoherent:

$$D(x, \gamma) = \int_{-\beta_0}^{\beta_0} \frac{\sin^2(2\pi Q(x+\beta+\gamma))}{(2\pi Q(x+\beta+\gamma))^2}\, d\beta \qquad 4.1.4$$

Finally, in order to obtain the entire intensity accumulated in the counter tube slit, we integrate with respect to γ:

$$D(x) = \int_{\gamma_0}^{\gamma} \int_{\beta_0}^{\beta} \frac{\sin^2(2\pi Q(x+\beta+\gamma))}{(2\pi Q(x+\beta+\gamma))^2} \, d\beta \, d\gamma \qquad 4.1.5$$

This integral can be represented by a power series, but the result is unfavorable for numerical treatment. The integral was evaluated for two wave lengths. Figure D.1.2 shows the measured direct beams for $\lambda = 8.3$ Å and for $\lambda = 1.9$ Å, together with the corresponding calculated theoretical diffraction profiles. As is evident, the lobes of the direct beam are satisfactorily explained by diffraction.

The nucleus is not correctly reproduced by this calculation. Evidently, the photographed focus is by no means homogeneous, so that deviations occur in the nucleus. The assumption of the Fraunhofer diffraction also is not strictly valid in the nucleus.

An analytic form of the direct beam which is as simple as possible is necessary for the fitting procedure described in Chapter D.3. It turns out that a good approximation to the measured points can be obtained by means of a linear combination of a Gaussian curve for the nucleus and a Lorenz curve for the diffraction halo (cf. Figure D.1.3).

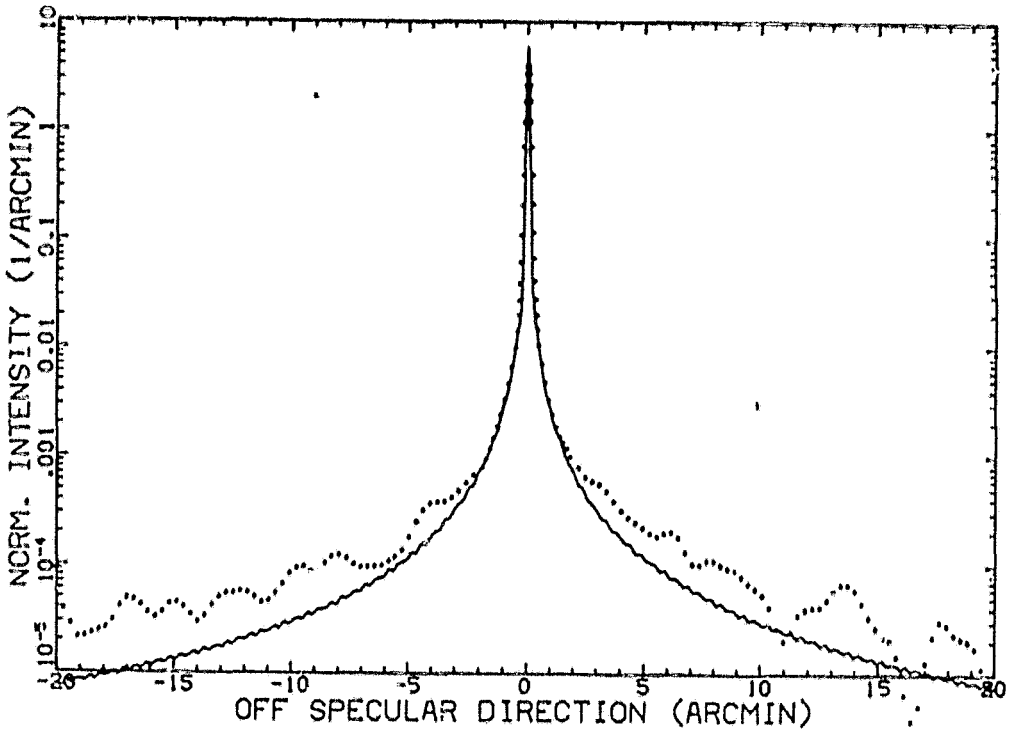

wavelength 8.3 Å

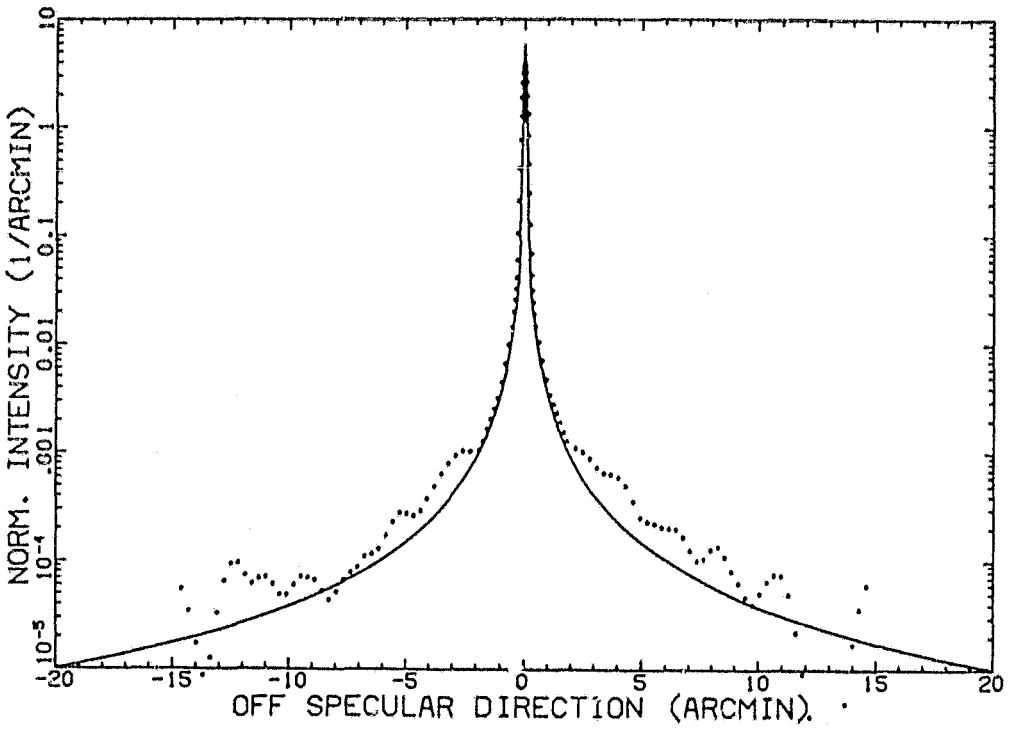

wavelength 1.9 Å

Figure D.1.2. The measured direct beam for two wavelengths and the corresponding calculated theoretical diffraction profiles.

$$D(x) = a\,G(x) + b\,L(x) \qquad 4.1.8$$

/39

where

$$G(x) = \frac{1}{\sqrt{2\pi}\,\theta_g}\,\exp\left(-x^2/2\,\theta_g^2\right) \qquad 4.1.9$$

$$L(x) = \frac{1}{\pi\,\theta_l}\,\frac{1}{1 + (x/\theta_l)^2} \qquad 4.1.10$$

$$a + b = 1 \qquad 4.1.12$$

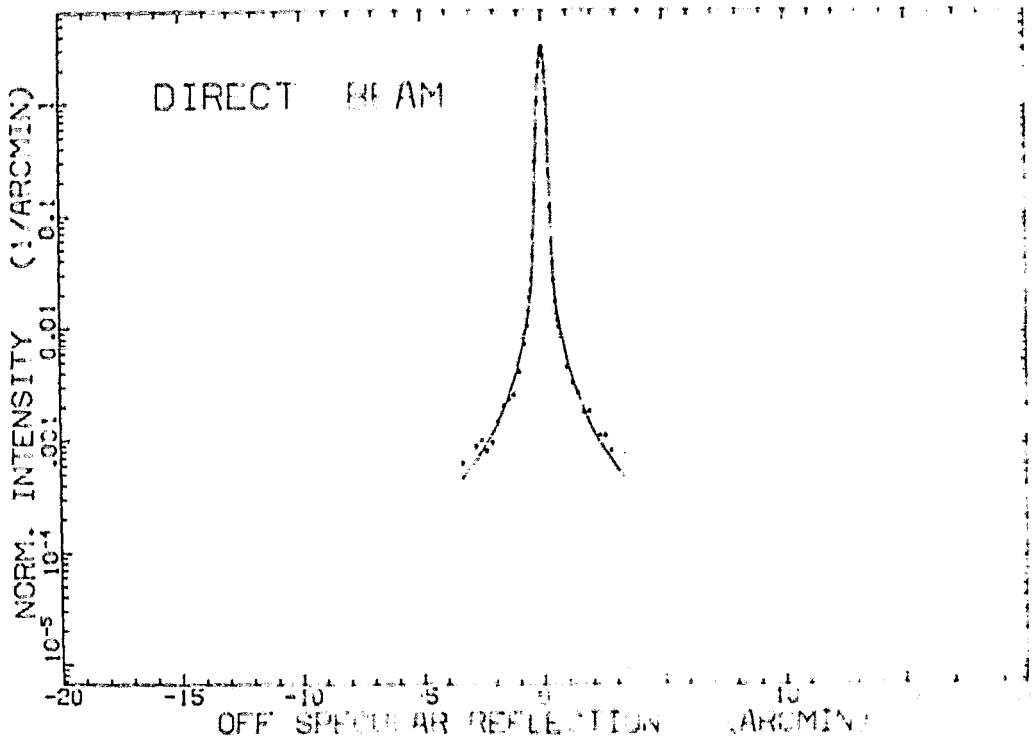

Figure D.1.3. The measured direct beam and the analytic curve fitted to it in accordance with 4.1.8.

TABLE V. The quantities which determine the direct beam

facility	θ_g [arcmin]	θ_l [arcmin]	a	b
PANTER	76.3	285	0.98	0.02
ZETA	86.1	145	0.95	0.05

D.2 The convolution of the direct beam and the scattering halo

In the derivation of the scattering distribution in B.2 and B.3 the point of departure was an incident plane wave. This breaks down in the specular delta-function, its Fourier transform. However, in the collimator geometry described in C.1, the direct beam is not plane but has an angle distribution treated in D.1. According to 4.1.8, it can be approximated by

$$D(\varphi) = a\,G(\varphi) + b\,L(\varphi) \quad \text{where} \quad a+b=1 = \int G(\varphi)\,d\varphi = \int L(\varphi)\,d\varphi$$

$$I(\varphi) = \frac{1}{I_r}\cdot\left(\frac{dI}{d\varphi}\right) = F_d\ \delta(\varphi) + F_s\,H(\varphi) \qquad 4.2.1$$

where

$$F_d = (1 - q_o);\ F_s = q_o;\ \int H(\varphi)\,d\varphi = 1.$$

The measured scattering distribution is now the convolution of the direct beam and the slit image function:

$$Str(\varphi) = I(\varphi) \oplus D(\varphi) \qquad 4.2.2$$

The convolution obeys the distributive law and preserves the norm:

$$Str(\varphi) = F_d\ (\varphi)\oplus D(\varphi) + F_s a H(\varphi)\oplus G(\varphi) + F_s b H(\varphi)\oplus L(\varphi) \qquad 4.2.3$$

The convolution of the delta function leaves an arbitrary function invariant:

$$\delta(x)\oplus f(x) = \int_0^\infty \delta(y)\,f(y-x)\,dy = f(x) \qquad 4.2.4$$

Since according to D.1, $b \ll a$ and $F_s \ll F_d$ hold (for small scattering), $F_s \cdot b$ is vanishingly small. From $F_s a = F_s(1-b) \approx F_s$ follows:

$$Str(\varphi) = F_d\,D(\varphi) + F_s\,H(\varphi) \oplus G(\varphi) \qquad 4.2.5$$

Here the first term represents the coherent reflected specular component and the second term corresponds to the incoherent scattered component. Now if the halo $H(\psi)$ has a much broader angle distribution than the nucleus of the direct beam $G(\psi)$, then $G(\psi)$ can be /40 approximated by $\delta(\psi)$, so that consequently, $G(\varphi)\oplus H(\varphi) = H(\varphi)$. Thus, the measured distribution can be represented finally as the sum of the direct beam and the halo:

$$Str(\Phi) = \Gamma_1 D(\Phi) + \Gamma_2 H(\Phi) \qquad 4.2.6$$

D.3 Curve fitting by the method of least squares /41

Despite the enormously small scattering component in the case of good samples--the intensity in the halo was situated in the neighborhood of 0.1 to 1 counts/sec--and the associated bad photon statistics, it was desirable to be able to make statements about the correlation lengths and to remove the error in determining the scattering component resulting from the exponential extrapolation in the nucleus.

For this purpose, a method was applied in which the exact slit image function was fitted to the measurement points of a single measurement, assuming an exponential autocorrelation function with different parameters σ and T. After the measurements were evaluated according to this method, it turn out that very different values of the parameters σ and T resulted from the individual measurements on a sample. Particularly in the case of measurements involving diffraction numbers smaller than 5 minutes of arc/Å--which were out of place even in the evaluation of the raw data--the microroughness was too high by a factor of 10 and the correlation lengths by a factor of 100. The removal of these uncertainties requires a procedure in which all the measurements on a sample are summarized in weighted form and σ,T are dealt with in a single parametric representation. Here we shall explain the most important program steps.

As shown in Chapter C.4, the mirror acts as a slit: In proportion to the projected surface, it screens out a part of the direct beam. Figure D.3.1 shows the geometry and the quantities used in the following analysis. It is assumed that beams whose divergence exceeds δ_o are not reflected from the mirror.

$$\tan \delta_o = \frac{D + SL \sin\alpha}{C} \qquad 4.3.1$$

/42

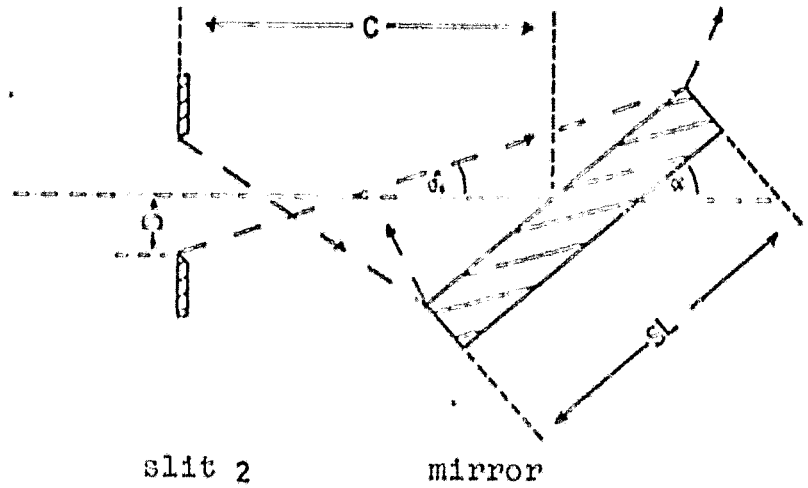

Figure D.3.1: Screening out the direct beam by the mirror

Therefore, in the program the intensity of the direct beam outside δ_o was equated to zero. Here a possible diffraction on the edges of the mirror and the integrating effect of the counter tube slit were neglected. Both effects produce a flatter decrease. It was also assumed that the mirror was symmetrically illuminated as a general principle.

Next, the measurement points (x(i), y(i)) were normalized in order to obtain a representation consistent with 2.4.3. For this purpose, the integral under the scattering curve was approximated according to the procedure described in Chapter C.1: The rectangles of height y(i) and width x(i+1)-x(i) were summed and subsequently extrapolated exponentially outwards. Then the counter rates y(i) were divided by the integral thus obtained.

Since normally the true maximum of the specular beam will not be attained exactly, a zero point displacement had to be fitted to the curves. On the average, this amounted to 0.1 minutes of arc which corresponds to approximately the half width of the direct beam.

/43

According to 4.2.6, the form of the direct beam must be reproduced exactly in the scattering curve. However, three different effects can cause a deformation:

If the collimator slit and the counter tube slit are not precisely parallel to each other, a widening of the beam can result. If the normal from the mirror to the plane defined by slit 2 and the counter tube slit has an inclination angle of $90°-\varepsilon$, then the image of slit 2 is tilted through an angle of 2ε in the counter tube plane. This, too, leads to a broadening of the specular beam. If the mirror has long-wave unevennesses (in the range SL/2), then the form of the direct beam is also changed. Statistical matching errors result in broadening, while concave mirrors constrict the nucleus. All three of the errors mentioned here appeared in the measurements so that it was necessary to introduce a deformation parameter, V. In this connection, it was assumed that only the variance of the Gaussian function defined in D.1 changes, whereas the diffraction-dominated halo of the direct beam does not change. In the case of the individual measurements, the parameter V ranged between 0.8 and 2.5. To be sure, it turned out that in the case of a bad adjustment of the sample (V=2.5), the Gaussian curve was not preserved and the nucleus in particular was no longer symmetrical. This led to a general error of circa 10% in determining the integral and the associated normalization.

To each measurement point y(i) was assigned an intrinsic error y_i, and the following error analysis was employed:
The normalized stray flux is determined in accordance with $y_i=(c-u)/s$, where c is the counter rate of the individual measurement point, u is the background in the given case and s is the integral over the measurement points. From the Poisson statistics of the counter rates, the statistical error of the individual measurement point amounts to:

$$y_i(\text{stat}) = \frac{1}{S}\sqrt{c + u + (c - u)^2 \frac{\Delta s^2}{s^2}} \qquad 4.3.2$$

y_i is compared with the theoretical curve:

$$\text{Str}_i = 4\, k^3\, \alpha^3\, \sigma^2\, T\, \sigma(1) \qquad 4.3.3$$

$\sigma(1)$ is a factor of order of magnitude 1 which can be neglected in this analysis; hence, it suffices to consider the error in the prefactors. An error in Str_i results:

$$\frac{\Delta Str_i}{Str_i} = 3 \sqrt{\frac{\Delta k^2}{k^2} + \frac{\Delta \alpha^2}{\alpha^2}} \qquad 4.3.4$$

Hence, the error in the individual measurement point is:

$$y_i = \frac{1}{s} \sqrt{c + u + (c-u)^2 \left(\frac{\Delta s^2}{s^2} + 9 \frac{\Delta k^2}{k^2} + \frac{\Delta \alpha^2}{\alpha^2}\right)} \qquad 4.3.5$$

As described above, $\Delta s/s$ is approximately 10%. The applied radiation was not purely monochromatic. The finite energy resolving power of the counter tube imposes the condition that the increments from the continuum radiation and other characteristic lines be admixed. The estimated error $\Delta k/k$ is about 8%. The error in the angle of incidence is determined by the adjustment procedure described in C.1. The mirror and the optical axis were parallel to within 1.5 minutes of arc. The calibration between the motor step width and the angle of incidence contains an error of 1%. According to C.4, time variations can be neglected.

Thus, a normalized measurement point has an absolute error amounting to

$$y_i = \frac{1}{s} \sqrt{c + u + (c-u)^2 \left(0.08 + 20.25 / \alpha^2\right)} \qquad 4.3.7$$

when the angle of incidence is expressed in minutes of arc.

Next, for the entire batch of measurements, a reduced chi-square formula was defined:

$$\chi^2_{red} = \frac{1}{f} \sum_{j=1}^{m} \sum_{i=1}^{n_j} \left(\frac{y_{ij} - f_{ij}}{\Delta y_{ij}}\right)^2 \qquad 4.3.8$$

where m is the number of measurements, n_j the number of measurement points in each case, and $f = \sum_{j=1}^{m} n_j - 2$ is the number of degrees of freedom.

In the parameter plane (σ,T), the distribution of the reduced chi-square was calculated and investigated for minima. For reasons to be discussed in Chapter D.6, only the measurement points outside of ±5 minutes of arc and only measurements with diffraction numbers 5 are minutes/Å were used. For a large number of degrees of freedom the probability distribution of the reduced chi-square converts into a Gaussian curve with mean value 1 and 1/e width $v = \sqrt{2/f}$. The distance of the calculated minimum X^2 from 1, measured in v units provides a measure of the goodness of the theoretical model used (Bevington 69).

Figure D.3.3 displays the chi-square contour lines in the (σ,T) plane in the case of the sample zerodur A. Here the minimum X^2 is 0.992 per degree of freedom which argues in favor of the correctness of the model used.

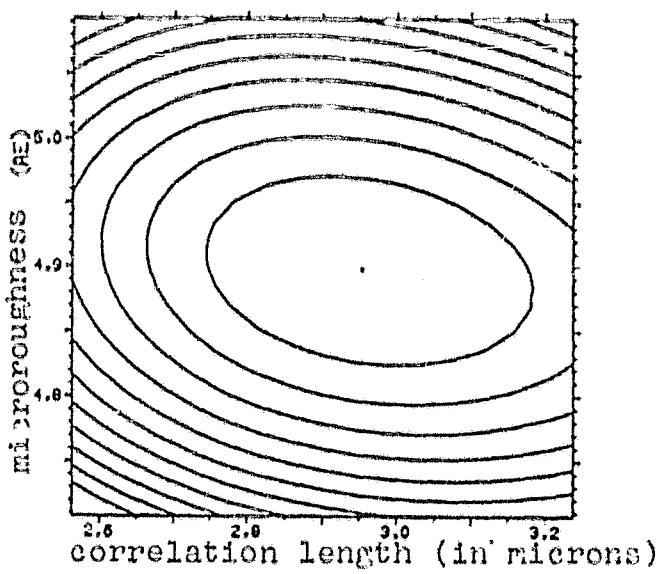

Figure D.3.3: The chi-square contour lines in the parameter plane (σ,T)

The value of $X^2_{red}(min)$ is not correspondingly good for all the samples measured. The deviations from 1 scatter between 0 and 5v. /46

The two innermost contour lines in Figure D.2.3 have the respective values $X^2_{red}(min) + 2.3/f$ and $X^2_{red}(min) + 4.6/f$

These two surfaces furnish the so-called 50% and 90% confidence range (Lampton 76). With a respective probability of 50% and 90%, the true values of the given parameters in the indicated ranges. Thus, we obtain for the first time a very good estimate for the error in the calculated surface parameters. In this (best) case, the results are:

$$\sigma = 4.9 \pm 0.1 \ \text{Å} \quad (2\%)$$
$$T = 2.0 \pm 0.3 \ \mu\text{m} \quad (10\%)$$

D.4 Various autocorrelation functions /47

For large-scale scattering ($g_o >> 1$) the scattering distribution is not simply proportional to the power spectrum of the surface, but the interrelationship in 2.2.6 must be resolved directly. Since we are here interested in only the slit image function of the mirror, we can integrate the point image function over γ:

$$\frac{1}{I_r}\left(\frac{dI}{d\varphi}\right) = \int \frac{1}{I_r}\left(\frac{dI}{d\omega}\right) d\gamma \qquad 4.4.1$$

Applying 4.4.1 to 2.2.6, we obtain on the right side the double integral:

$$I_c(\varphi) = \iint J_o(v_{xy}\tau)\,d\gamma\; C^m(\tau)\,\tau\,d\tau \qquad 4.4.2$$

For $\alpha, \psi << 1$, the argument of the Bessel function v_{xy} can be replaced by (cf. 2.2.2):

$$v_{xy} = k\sqrt{a^2 + \gamma^2} \qquad 4.4.3$$

where a is defined by

$$ka = k\,\varphi(\alpha + \varphi/2) = v_x(\gamma = 0) \qquad 4.4.4$$

Then in 4.4.2, the integration over τ can be carried out:

$$I_c = \frac{1}{K}\int \cos(\tau ka)\; C^m(\tau)\; d\tau \qquad 4.4.5$$

This integral, which is a kind of Fourier transform of higher order, will be computed in the sequel for various autocorrelation functions:

1. From an exponential autocorrelation function (2.4.4), we obtain: /48

$$I_c = \frac{T\pi}{mk} \frac{1}{1+(\frac{kaT}{m})^2} \qquad 4.4.6$$

2. From a Gaussian type autocorrelation function (2.4.5), we obtain:

$$I_c = \frac{\sqrt{\pi}\,T}{2\sqrt{m}} \exp(-(\frac{kaT}{2\sqrt{m}})^2) \qquad 4.4.7$$

3. From a Lorenz-type autocorrelation function:

$$C(\tau) = \frac{1}{1+(\tau/T)^2}$$

there results

$$I_c = T \frac{\exp(-Tk|a|)}{(m-1)!\ 2^{2m-1}} \sum_{l=0}^{m-1} \frac{(2m-l-2)!\,(2Tk|a|)^l}{l!\ (m-l-1)!} \qquad 4.4.8$$

Then the total slit image function is described by:

$$\frac{1}{I_r}(\frac{dI}{d}) = e^{-g}\left\{ \delta(\varphi) + \frac{2\pi F^2}{A} \sum_{m=1}^{\infty} \frac{g^m}{m!} I_c(\varphi) \right. \qquad 4.4.9$$

according to 2.2.6. The measurements on the bad sample 38A described in C.2 were processed according to the procedure described in D.3 where for each of the three different estimates, the exact slit image function according to 4.3.9 was applied. A X^2-test showed that the data of the entire batch of measurements could be well represented by an exponential autocorrelation function, while a Gaussian-type or Lorenz-type correction can be excluded.

Table V shows the results of this comparison. For each of the assumed autocorrelation functions, the optimum surface parameters are found in columns 2 and 3, and the minimum X^2 attained is in column 4.

/49

Figure D.4.1, using the example of a measured scattering distribution, shows the optimum curves for the respective autocorrelation functions. The scattering distribution is best approximated by the curve generated by an exponential correlation. The deviations for small scattering angles ($\alpha \lesssim \varphi$) are caused by shading effects.

autocorrelation functions	σ[Å]	T [μm]	χ^2_{red}(min)
Gaussian-type	61± 19	4 ± 3	5.17
exponential	86± 10	11 ± 6	1.50
Lorenz-type	68± 22	4 ± 2	3.38

Table V: χ^2-test for various autocorrelation functions.

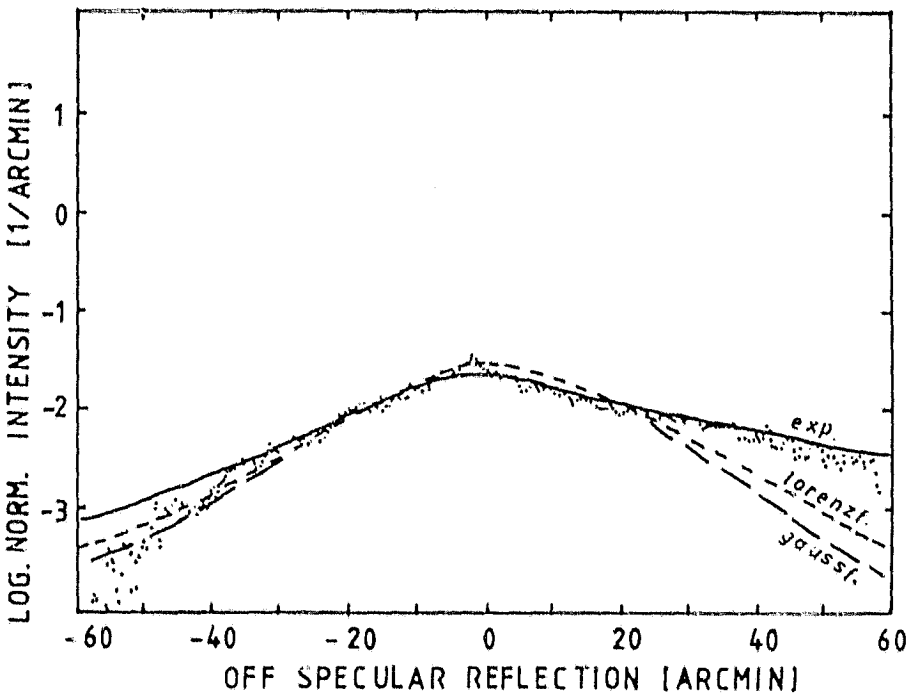

Figure D.4.1: The measured scattering distribution for the sample 38A with α = 60 arcminutes, λ=8.3 Å, and the theoretical curves fitted to it for various autocorrelation functions.

D.5 Results of the fitting procedure for small scattering

In the special case of small scattering ($g_o << 1$), the simple expression for the slit image function according to 2.4.3 can be used. Assuming an exponential autocorrelation function, the one-dimensional power spectrum $W_1(v)$ can be read off directly from 2.4.6. Taking into account 4.2.7 and 4.4.4, we have finally:

$$\frac{1}{I_r}\left(\frac{dI}{d\varphi}\right) \quad (1-q_0)D(\varphi) + 4\pi^3 \alpha(\alpha+\varphi)^2 \frac{\bar{T}}{\pi} \frac{1}{1+(k\alpha\bar{T})^2} \qquad 4.5.1$$

When this slit image function is used with the fitting procedure described in Chapter D.3, then a parametric representation can be found for each measured sample with sufficient statistics which is a good fit in the stray lobes for diffraction numbers smaller than 5 minutes of arc/Å. The screening of the direct beam described in D.3 is again to be found in the measurements. In some curves, even an asymmetric illumination can be detected.

In summary, it can be stated here that the stray lobes beyond ±5 minutes of arc in the case of microroughness down to 2.5 Å, and for all energies used, can be very well described by the surface scattering theory with an exponential formulation for the covariance function. The resulting microroughness and correlation lengths are presented in Table VI and Figure D.5.1. Assuming a uniform correlation length for all samples, we find: $\bar{T} = 2.3 \pm 0.6$ µm. Some examples of measured scattering curves and the theoretical distributions fitted to them are shown in Figure D.5.2.

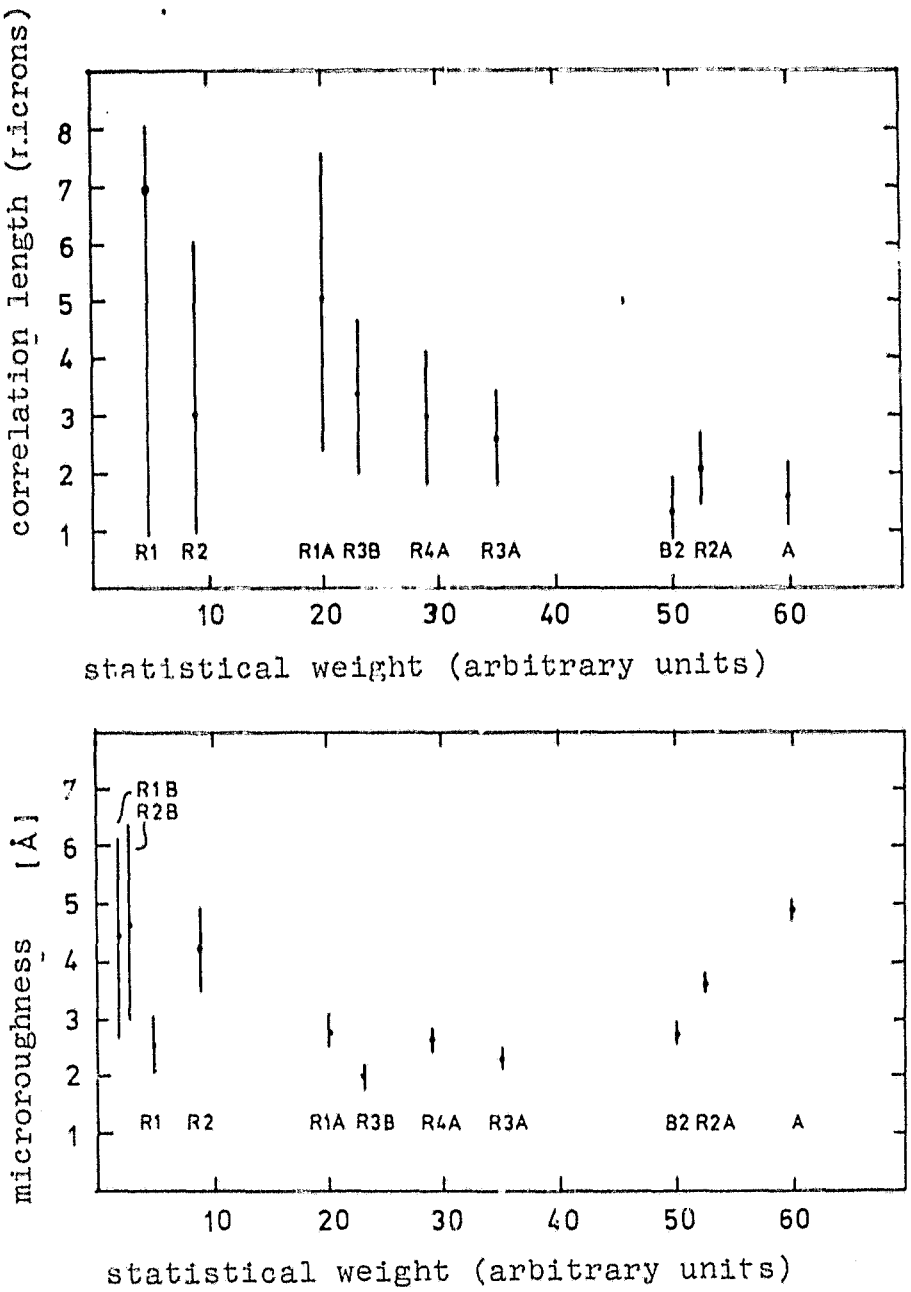

Figure D.5.1: Summary of the results of the fitting procedure for all zerodur samples plotted against the statistical weight of the individual measurement series.

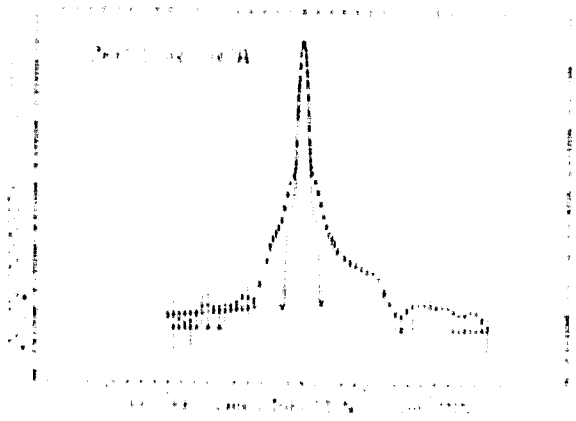

angle of : 15 arcmin
incidence

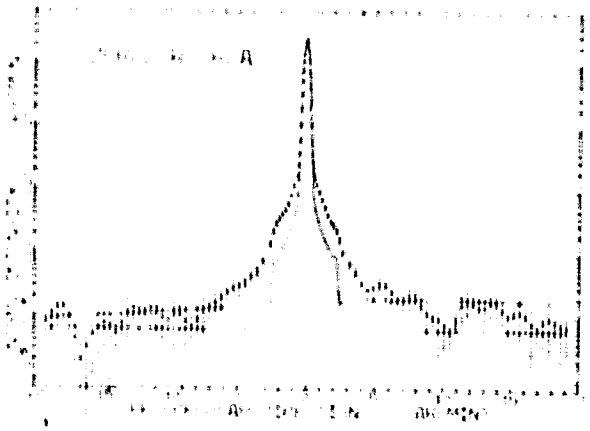

angle of 30 arcmin
incidence

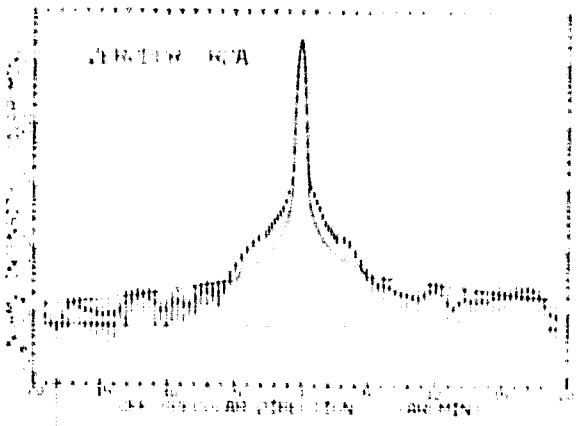

angle of : 60 arcmin
incidence

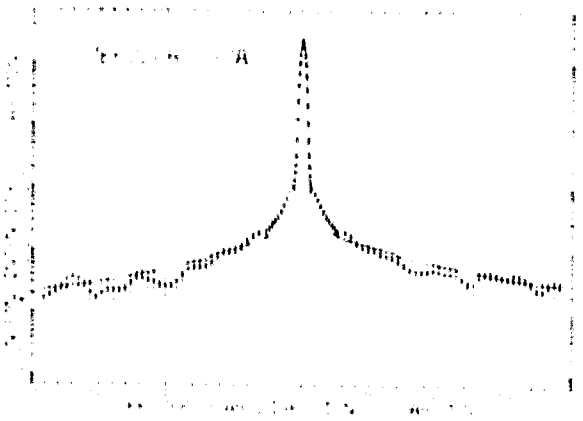

angle of : 90 arcmin
incidence

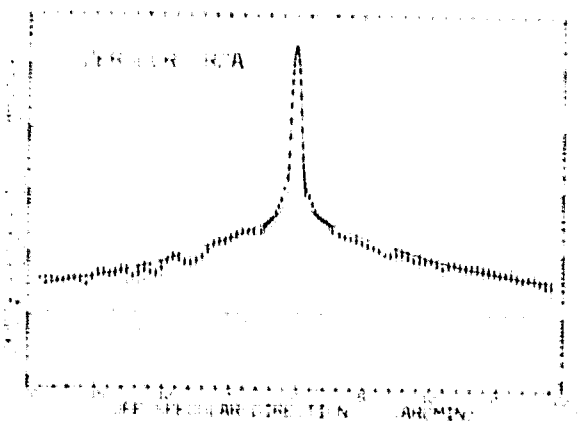

angle of : 120 arcmin
incidence

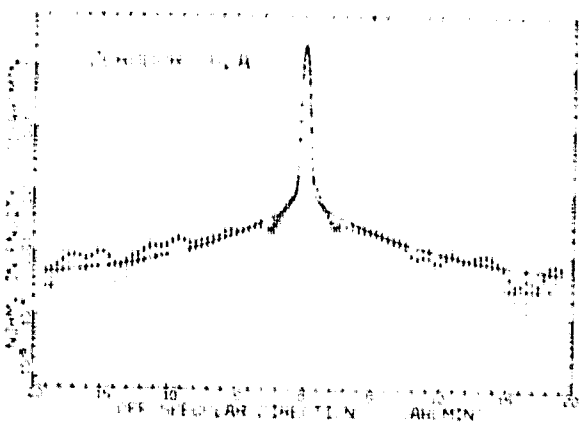

angle of : 150 arcmin
incidence

Figure D.5.2: Some examples of measured scattering distributions and the theoretical curves fitted to them for the same R2A when λ = 8.3 Å, σ = 3.8 Å, T = 2.0 µm

sample	roughness [Å]	correlation length [µm]
disk 1	2.6 ± 0.5	7 ± 6
disk 2	4.3 ± 0.7	3 ± 3
Zerodur A	4.9 ± 0.1	2.9± 0.3
Zerodur R1A	2.9 ± 0.3	5.0± 2.6
Zerodur R2A	3.8 ± 0.1	2.0± 0.6
Zerodur R3A	2.4 ± 0.1	2.6± 0.7
Zerodur R3B	2.3 ± 0.2	3.4± 1.4
Zerodur R4A	2.7 ± 0.1	3.0± 1.1
Zerodur B2	2.7 ± 0.1	3.0± 1.1

Table VI: Results of the fitting procedure

D.6 Deviations in the kernel of the scattering distribution /54

In this chapter, we shall consider in detail the ranges $\psi < \pm$ 5 arcmin and $\alpha/\lambda <$ 5 arcmin/Å which were excluded in D.4. As can be seen in Figure D.5.2, in a range of several minutes of arc, the measured points in all cases lie above the calculated curves. The resulting triangle, as will be shown, cannot be explained by scattering.

First of all, we shall attempt to represent the dependence on the parameters angle of incidence and wavelength. The effect is to be characterized by the following quantities: S_e specifies the relative intensity in %, and θ is the 1/e-width in minutes of arc. In order to express the characteristic quantities, the excess intensity was characterized by a Gaussian curve, whose parameter was fitted to the measured points, while the optimal quantities σ and T, determined according to Chapter D.5, were held fixed. If θ is smaller than circa 0.5 minutes of arc, and if S_e is smaller than circa 10%, then the excess disappears under the specular reflected beam and its characteristic quantities can only be determined as

upper limits. The results of this procedure are presented in Table VII.

Due to the meager information about this effect, the poor photon statistics, the limited resolution in the nucleus, and the possibly non-optimum fitting by means of a Gaussian curve, the spectrum of the results is varied. However, by way of summary, we can say: The 1/e-width is in no instance substantially greater than 2 minutes of arc and the relative intensity does not exceed 3%. When the wavelength is constant, S_e increases somewhat as the angle of incidence decreases, while θ remains approximately constant. For the wavelengths 8.3 Å and 13.3 Å, the behavior is approximately the same, while in the case of small wavelengths, the triangle seems to disappear, or θ becomes so small that the excess intensity is hidden under the specular reflected beam.

/56

In order to be able to make somewhat more precise statements, I have averaged the available quantities from Table VII over the various angles of incidence and the different samples and have thus obtained the generalized quantities $S_e(\lambda)$ and $\theta(\lambda)$:

wavelength [Å]	13.3	8.3	2.8	2.4	1.9
$S_e(\lambda)$ [%]	1.6	1.7	1.6	?	?
$\theta(\lambda)$ [arcmin]	0.9	1.1	0.4	0.3	0.5

A possible interpretation of these results is that the intensity of this excess is always approximately equal in size, and only the angle distribution varies with the energy, i.e., becomes smaller with larger energies. If we assume that approximately 10% of the triangle,=i.e., about 0.2% of the relative intensity outside of ± 2 minutes of arc will be seen, then the scattering distribution for $\alpha/\lambda<5$ arcmin/Å is dominated by the nucleus: The smaller the surface scattering, the more the nucleus grows. This is how we can also understand the increase in the "microroughness" when the

TABLE VII. The characteristic quantities of the triangle.

s : the relative surface in %

θ : the variance in minutes of arc

the diffraction numbers decrease, as was described in Chapter C.4.

A similar triangle is also visible in the case of other samples and other test assemblies. Thus, similar effects, which are not explanable by the scattering theory, have shown up in Lenzen's and my measurements on the sample 38A (Lenzen 78, C.1), the calibration measurements on the 32 cm Wolter telescopes (Ondrusch 78), as well as the calibration measurements in Huntsville (Zombeck 80) on one of these 32 cm telescopes.

/57

Next, we shall discuss some mechanicms which could be utilized to explain the observations in question. In particular, these are:

1. A second scattering distribution in the nucleus;
2. Tangent errors;
3. Thomson scattering;
4. Shading and multiple reflections;
5. Inadequacies in the test assembly.

Re 1: The surface could possess a second component of the roughness which is dominant for small diffraction numbers and which is hidden in some way under the nucleus when the diffraction numbers are larger so that it simulates the constancy described above. We shall now show that this is not the case.

According to 2.4.3, in the limiting case, the following condition must hold for any two scattering distributions:

$$I(k\alpha, \varphi) = c^3 \, I(c\, k\alpha, \varphi/c) \qquad 4.5.1$$

Where I denotes the stray halo of the slit image function and c denotes the ratio of the two diffraction numbers. Random tests when measuring small diffraction numbers have shown that this condition is not satisfied, i.e., that the excess intensity is, therefore, not caused by scattering.

Re 2: The obvious explanation for the triangle in the nucleus would be a reflection on the unevennesses of the surface due to the beam

optics. In this case, the distribution of the surface gradients would be expressed with doubled width in the split image function. According to the results from Table VI, we should thus expect that about 2% of the surface would have a gradient distribution with a width of circa 0.5 minutes of arc. In optics such effects are known as so-called matching errors, deviations from a plane surface which impair the resolving power of a mirror by broadening the specular δ-function. In order to study their influence on the scattering distribution in the x-ray range, such matching errors were measured in several mirrors. For this purpose, the interferences of /58 equal thickness were determined on some mirrors using a Fizeau Interferometer from the firm of Carl Zeiss. Figure D.6.1 shows these interference specimens for two samples. From the bending of the bands, we can conclude directly the extent of the deviation of the surface from the plane in units of the length of the incident wave. In the most unfavorable case (on the left in the figure: zerodur A), this is about 1μm. When the correlation length is circa 50 mm (half the length of the sample), there is a maximum rise of about 5 seconds of arc. In the case of the other measured samples (to the right in the figure: disk 3), the matching errors were at most 1 second of arc. The interference figures do not change when the samples are clamped in the holder provided.

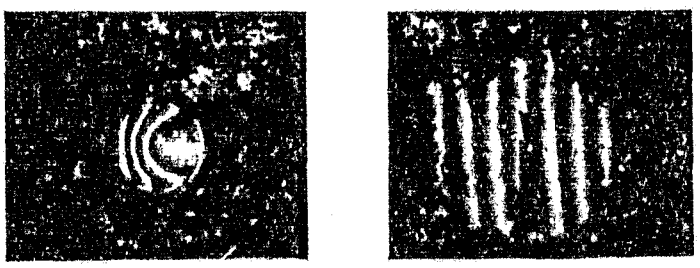

Figure D.6.1: Interferences of equal thickness in the case of two samples, using an He-Ne laser (from the firm of C. Zeiss, Oberkochen). On the left: zerodur A; on the right: zerodur disk 3.

The vertical resolution for this method is circa 500 Å, the later 1, circa 1 cm. Thus, matching errors in the conventional sense cannot be responsible for the triangle in the nucleus. The

cause lies rather in the order of magnitude of the direct beam divergence. However, no statement is made concerning tangent errors which are smaller than the lower limits stated above.

/59

Re 3: The remaining possible explanations are somewhat more far-fetched, and provide only indirect hints about the nature of possible deviations from the scattering theory. However, for the sake of completeness, they are also enumerated here.

In order to estimate the Thomson scattering, the effective cross-section of x-ray radiation on gold atoms is analyzed. The scattering cross-section for a single electron is about 0.6 barn at 1 keV. It increases approximately as Z^2, so that for gold se obtain a value of 3.7×10^3 barn/atom, which is consistent with the effective cross-section for coherent scattering of 4.0×10^3 barn/atom (Atomic Data 73). When this is multiplied by the density of gold, we obtain a diffusion coefficient of $\mu = 240$ cm^{-1}. Lenzen (Lenzen 78) calcualted a penetration depth of circa 20 Å over a wide range of wavelengths and incidence angles. However, the actual distance, s, which is covered in the material is 20 Å/tan α. Thus, in the case of an incidence angle of 15 minutes of arc, s is about 4000 Å. Hence, the intensity of the scattering into the half-space is 0.55% at 1 keV. Analogously 1.44% scattering intensity is obtained at 10 keV. However, since Thomson scattering is distributed quasi-isotropically, the portion falling into the observed solid angle is only 10^{-7}. Therefore, bulk scattering can be neglected in comparison to small-angle scattering, whereas in the integral reflectivity, it must definitely make itself felt.

Re 4: In order to estimate the possible consequences of shading effects and multiple reflections of an equal order of magnitude, the Parthometer measurement described in B.5 was analyzed. A beam tracking program calculated for each given angle of incidence, the illuminated parts of the surface, its vertical distribution and correlation function. It turned out that the normally distributed surface is again normally distributed in the case of partial shading, although the width of the distribution (and thus the microroughness)

becomes somewhat smaller in the case of a decreasing angle of incidence. The correlation length as well as the mean value of the surface increase then. However, significant shading effects first showed up beginning with an incidence angle of circa 15 /60 minutes of arc, about five times the rise derived from the surface parameters. Since the anticipated rises in the case of the well polished samples were situated still lower, the shading and multiple reflection effects cannot play any larger role in the nucleus. On the other hand, the deviations visible in Figure D.4.1 for small reflection angles can be traced back to shading effects.

Re 5: The inadequacies in the test assembly described in C.4, especially the possible stray light in the installation could be the cause of deviations. As described in C.4, the test assembly at the ZETA facility was substantially improved. With the changed layout the sample zerodur A was measured a second time. The comparison of the data obtained with different facilities and a different test assembly discloses two things:

1. When the diffraction numbers are greater than 5 minutes of arc/Å, the scattering curves as well as the microroughness and the correlation lengths determined by the fitting procedure are equal within the limits of measurement accuracy.
2. For small diffraction numbers, there are no possibilities of direct comparison; however, the excess intensity could be somewhat high[illegible] for the measurements made at the ZETA facility.

Besides the proof of the reproducibility of the scattering measurements, the conclusion is admissible that the deviations in the nucleus were not caused by the inadequacies in the test assembly described in C.4. The triangle in the nucleus appears, however, to depend on the geometry involved in the layout of the test assembly.

E. Summary /61

With the two x-ray test facilities ZETA and PANTER of the MPE, 170 scattering measurements were on 14 plane mirror samples at wavelengths between 13.6 Å and 1.9 Å and for incidence angles between 5 and 150 minutes of arc. The slit image function was measured chiefly for reflection angles between ±20 minutes of arc.

It turned out that the fundamental goals of this research, namely, on the one hand to improve the diagnosis of measurements of rough surfaces, and on the other hand, to investigate the possibility of a bench test of the 80 cm telescope at high energies, and whether both objectives could be pursued with the same means. If e.g., we increase the incident photon energy, i.e., if we reduce the wavelength of the incident waves, then we become sensitive to smaller structures on the surface. Like all diffraction processes, scattering is also dependent solely on the ratio of the angle of incidence to the wavelength. In the text, this ratio is called the diffraction number. However, since the critical angle of the external total reflection of x-ray beams is approximately proportional to the wavelength, as the wavelength decreases, the incident beam must be flatter in order to obtain sufficient reflectivity, i.e., the diffraction number remains approximately constant. Thus, no improvement in diagnosis is possible via higher energies.

Nevertheless, to attain both goals, as broad gage a measurement program as possible was set up. On as many samples as possible, small as well as large incidence angles and wavelengths were suitably permuted. In order to obtain good photon statistics even in the case of well polished samples, it was necessary to extend substantially the time spent in the measurement process.

To describe the x-ray scattering measurements, the Raleigh vector perturbance theory was used after it had been determined that with regard to the special case of small roughness involved in this paper, the vector perturbance theory is equivalent

to the scalar surface scattering theory used in the previous papers from this institute. The basic assertion of both theory is that the point image function is directly proportional to the power spectrum of the surface. /62

In order to evaluate the series of measurements, a procedure was developed in which all measurements on a sample were collectively weighted and treated with a single parametric representation for microroughness and correlation length. A detailed error analysis makes it possible for the first time to determine together with the microroughness the correlation length of a sample also as well as the error in the two surface parameters.

Clearly, the most important finding of this research is the conclusion that the results obtained for low energies (0.9-1.5 keV) are in good agreement with the results obtained with high energies (4.5-6.5 keV), provided that the diffraction numbers are larger than circa 5 minutes of arc/Å. Under these assumptions, the scattering properties of a telescope measured in the air in a shop test should be entirely comparable with the properties manifest in the subsequent range of application.

In the case of small diffration numbers, an effect showed up which casts new light on the rating of x-ray mirrors by means of their scattering properties. In the range between $\psi = \pm 5$ minutes of arc the measurement points lie without exception above the calculated curves. The residues can be characterized by Gaussian curves whose intensity and angle distribution are only weakly dependent on wavelength and angle of incidence. Therefore, the excess intensity cannot be explained by scattering. This effect is important, since on the one hand, the expected astrophysical dust dispersion halos lie in the same angle range (H. Spielgelhauer, private communication), and on the other hand, the resolving power of the mirror can be reduced by the continuing excess intensity under the nucleus. /63

A valid and cogent explanation for this effect still does not exist. The most obvious interpretation remains as before a reflection from long-wave irregularities (correlation lengths between 10 μm and 1 cm), whose flanks are circa 1 minute of arc steep. More precise information about the nature of this effect could result from a very exact two-dimensional measurement of the nucleus. Such an investigation is in preparation at the present time at the MPE. Unfortunately, it falls timewise outside the scope of the present paper. In order to clarify the range of the power spectrum which is inaccessible to both optical and x-ray optical measurements, it would be desirable to make a sensitive Perthometer measurement of a well-polished sample (Bennet 1979). In order to accomplish this, it would be necessary to improve the technology of stylus measurements.

For the encouragement to undertake this research, for his continuing interest and not the least, for the opportunity to carry out this work at the Max Planck Institute for Extraterrestrial Physics, I express my thanks to Prof. Dr. J. Truemper.

Especial thanks go to Dr. H. Bräuninger for the intensive care and helpful collaboration which he accorded me and this research.

I am also especially indebted to Dr. B. Aschenbach for fruitful discussions and critical perusal of my manuscript, and to Messrs A. Ondrusch, Dipl. Phys. and K. H. Stephan, Dipl. Phys. for their helpful participation in the scattering measurements.

I wish to express my hearty thanks to the entire x-ray group of the MPE, especially Dr. H. Fink, Dr. H. Haerle, Dr. P. Presdehl, H. Spiegelhauer, Dipl., Phys., and L. Wuestefeld, Dipl. Phys., for their friendly reception and interesting discussions.

REFERENCES

Aschenbach, B., Braeuninger, H., Stephan, K. H., Truemper, J: Proc. SPIE, 184, 234, (1979)

Atomic Data, 5, 49, (1973)

Barrick, D. E.: Radar Cross Section Handbook, Plenum Press, New York, (1970)

Beckmann, P., Spizzichino, A.: The Scattering of Electromagnetic Waves from Rough Surfaces, Pergamon Press, New York, (1963)

Bennet, H. E., Porteus, J. O., J. Opt. Soc. Am., 51, 123, (1961)

Bennet, H. E. Proc. SPIE, 184, 153 (1979)

Bevington, P. R.: Data Reduction and Error Analysis for the Physical Sciences, McGraw-Hill, New York,(1969)

Bowyer, C. S., Byram, E. T., Chubb, T. A., Friedmann, H.: Science 146, 912, (1964)

Carniglia, C. K.: Opt. Eng., 18, 104, (1979)

Church, E. L., Jenkinson, H. A., Zavada, J. M.: Opt. Eng. 18, 125, (1979a)

Church, E. L.: Proc. SPIE, 184, 196, (1979b)

Eastman, J. M., Baumeister, P. W.: Opt. Comm., 12, 418, (1974)

Elson, J. M. Bennet, J. M.: J. Opt. Soc. Am., 69, 31, (1979)

Garcia, N., (1979), to be published

Garibaldi, U., Levi, A. C., Spadacini, R., Tommei, G. E.: Surface Sci., 48, 649, (1975)

Giacconi, R., Rossi, B. B.: J. Geophys. Res., 65, 773, (1960)

Giacconi, R., Gursky, H., Paolini, F. R., Rossi, B. B.: Phys. Rev. Letters, 9, 439, (1962)

Hill, N. R., Celli, V.: Surface Sci., 75, 577, (1978)

Lampton, M., Margon, B., Bowyer, C. S.: APJ, 208, 177, (1976)

Lenzen, R.: Dissertation Tuebingen, (1978)

Ondrusch, A.: Master's Dissertation, Muenchen, (1978)

Rayleigh, Proc. Roy. Soc., A79, 399, (1907)

Truemper, J., Aschenbach, B., Braeuninger, H.: Proc. SPIE, 184, 12, (1979)

Wolter, H.: Ann. Physik, 10, 94, (1952)

Zombeck, M. V.: Proc. SPIE, 184, 49, (1979)

Zombeck, M. V.: Memorandum, (1980)